

**A Promising New Optical Nanoprobe for Cellular Imaging: Amine Passivated Fluorescent
Carbon Dots**

Adryanne Clermont-Paquette

A Thesis
In the Department
of
Biology

Presented in Partial Fulfillment of the Requirements
For the Degree of
Master of Science (Biology) at
Concordia University
Montreal, Quebec, Canada

December 2022

© Adryanne Clermont-Paquette, 2022

CONCORDIA UNIVERSITY

School of Graduate Studies

This is to certify that the thesis prepared

By: Adryanne Clermont-Paquette

Entitled: A Promising New Optical Nanoprobe for Cellular Imaging: Amine Passivated Fluorescent Carbon Dots

and submitted in partial fulfillment of the requirements for the degree of

Master of Science (Biology)

complies with the regulations of the University and meets the accepted standards with respect to its originality and quality.

Signed by the final Examining Committee:

_____ External Examiner

Dr. Pat Forgione

_____ Examiner

Dr. John Capobianco

_____ Examiner

Dr. Christopher Brett

_____ Supervisor

Dr. Alisa Piekny

_____ Co-Supervisor

Dr. Rafik Naccache

Approved by

Dr. Robert Weladji, Graduate Program Director

December 16th, 2022

Dr. Pascale Sicotte, Dean of Faculty of
Arts & Science

Abstract

A Promising New Optical Nanoprobe for Cellular Imaging: Amine Passivated Fluorescent Carbon Dots

Adryanne Clermont-Paquette

Concordia University,

Carbon dots (CDs) have garnered significant attention in the past decade owing to their fascinating luminescent properties and potential use in cell and tissue imaging, as well as for the study of biological processes. These quasi-spherical amorphous carbon-based nanomaterials can be tailored to emit light from the UV-NIR regions of the spectrum while offering low cytotoxicity and good biocompatibility. The physico-optical and -chemical properties of CDs are determined by the precursors, methods of preparation, and reaction conditions. These properties then influence their cellular uptake, cytotoxicity, and sub-cellular localization.

In this work, CDs synthesized from citric acid and five different amine passivating agents were characterized to reveal their properties, and determine how these properties affect their uptake and localization in cultured human cells (HFF-1; human male foreskin fibroblasts, and HeLa; human female cervical carcinoma). All CDs exhibited fluorescence with a corresponding max λ_{ex} at 350 nm and max λ_{em} at 450 nm. We found that these spherical amine passivated CDs ranged in size from 1.29 to 2.74 nm, and each had similar functional groups such as carboxyl, amines and amides. There was an increase in surface charge from -21 mv to +8 mv that correlated with the increase in amine passivation. All of the CDs had low cytotoxicity in both HFF-1 and HeLa cells, with an increase in uptake that correlated with an increase in their surface charge. While all of the CDs localized to the lysosomes, suggesting entry and trafficking via the endomembrane system, there was a difference in their enrichment; PH6-CDs (with the most amine-passivation) were the most strongly co-localized with lysosomes in both cell lines. Interestingly, DT3-CDs also localized to the cytosol, which could be explained by their amphiphilic properties causing (some) CDs to enter cells passively. These findings indicate that CDs could be made to have diverse optical properties and subcellular localization, which could be explored for applications as bioimaging nanotools, and/or delivery agents.

Acknowledgements and Dedications

I thank Dr. Alisa Piekny and Dr. Rafik Naccache for giving me the opportunity to study in their lab. My journey started as a volunteering undergraduate in Dr. Naccache's lab where I had the opportunity to grow as a scientist and learn all about these fascinating fluorescent carbon dots. Without this opportunity, completing a master's thesis would have never been possible. Thank you, Alisa and Rafik, for your patience, trust, constant input, generosity and for accepting me as a Biol 490 which gave me the opportunity to grow as a biologist and to continue as a graduate student in your lab. I am grateful for the time you both gave me, and all the hard work you put in to guiding my projects, both your individual strengths and knowledge made this research project an incredibly pleasant learning experience. Thank you for challenging me constantly to be a better scientist.

I thank my committee members, Dr. John Capobianco, Dr. Christopher Brett for their time and consideration. I thank you for the invaluable insight you have provided to this project.

I am very grateful to Dr. Chris Law, the operations manager of the *Centre for Microscopy and Cellular Imaging* (CMCI) at Concordia. Thank you for teaching me how to operate the CMCI's intimidating microscopes and for helping me through instrumental crises and for your incredible problem-solving skills and all the mini crash courses you gave me throughout the years.

I would like to thank the past and present members of both the Piekny and Naccache lab for all their help, time, and insight. Thank you, Jun-Ray Macairan, for mentoring me and introducing me to the world of carbon dots and for teaching me everything I needed for this project to be a success. I would also like to thank Kevin Larocque, working with you has been a joy. Thank you for all our bad and good times with the microscope, which has constantly been a challenge. Your constant help and guidance were and still are greatly appreciated. Thank you Tayline Medeiros, for your support and all your help, especially writing this thesis and helping with the instrumentations and figure making. Your constant positive attitude and your friendship means the world to me. And an overall thank you to all the other members that at one point or another helped with some experiments or simply answered one of my questions or had a great conversation with me.

Lastly, I would like to thank my parents, although to this day still have no clue what it is I am doing. Science is not for everyone, but they still asked questions and listened to me blathering about my passion. Without their support and their constant pushing I would certainly not have

gotten through these years. They have educated me to be this strong, independent, genuine, career-oriented and the businesswoman that I am. Thank you dad for taking me on our business journey and teaching me how to be successful and thank you mom for being my confidante. Love you both very much.

Table of Contents

Lists of Figures	iv
List of Abbreviations	v
Chapter 1. Introduction	1
1.1. The power of nanoparticles	1
1.2. Bioimaging at the nanoscale.....	1
1.3. Introduction to CDs	4
1.4. CDs as bioimaging nanotools.....	6
1.5. Addressing the Gap	10
1.6. Objectives.....	10
Chapter 2. Materials and Methods	11
2.1. Chemicals and reagents	11
2.2. Synthesis of carbon dots	11
2.3. Fluorescence spectroscopy	11
2.4. UV-vis Absorbance Spectroscopy.....	12
2.5. Fourier Transform Infrared Spectroscopy	12
2.6. Transmission Electron Microscopy	12
2.7. Quantum Yield	12
2.8. Zeta-Potential.....	13
2.9. Photobleaching of CDs.....	13
2.10. Cell Culture.....	13
2.11. Cytotoxicity.....	14
2.12. Microscopy	14
2.13. Statistical Analysis.....	15

Chapter 3. Results	16
3.1. Optical properties of amine-passivated CDs	16
3.2. Physicochemical properties of amine-passivated CDs	16
3.3. Cytotoxicity of amine-passivated CDs	20
3.4. Cellular uptake of amine-passivated CDs	23
3.5. Subcellular localization of amine-passivated CDs	23
Chapter 4. Discussion	29
Chapter 5. References	32
Appendix 1	38

Lists of Figures

Figure 1. Quantum dots and their relative energy and fluorescence	12
Figure 2. Graphical representative of carbon core- and molecular-state fluorescence Mechanism.....	14
Figure 3. Uptake of nanoparticles in human cells	17
Figure 4. Optical properties of amine-passivated CDs	26
Figure 5. The surface composition and charge of amine-passivated CDs	28
Figure 6. TEM images of squasi-spherical amine-passivated CDs	29
Figure 7. Photostability of amine-passivated CDs under 365 nm light exposure.....	30
Figure 8. Cell viability assessment of amine-passivated CDs in HFF-1 and HeLa cells.....	33
Figure 9. Cellular uptake of CDs in HFF-1 and HeLa cells.....	34
Figure 10. CDs co-localization to the lysosomes and the cytosol in HFF-1 cells	36
Figure 11. CDs co-localization to the lysosomes and the cytosol in HeLa cells	37

List of abbreviations

UV-vis	ultraviolet-visible
CDs	Carbon dots
QDs	quantum dots
UCNPs	upconverting nanoparticles
AuNPs	gold nanoparticles
LDH-NPs	Layered double hydroxide nanoparticles
NPS-NPs	polystyrene nanoparticles
NIR	near infrared
NPs	nanoparticles
TEM	transmission electron microscopy
XPS	X-ray photoelectron spectroscopy
FT-IR	Fourier-transform infrared
XPS	X-ray photoelectron spectroscopy
HFF-1	human male foreskin fibroblasts
HeLa	human female cervical carcinoma
ER	endoplasmic reticulum
DMEM	Dulbecco's Modified Eagle Medium
PBS	phosphate buffered saline
FBS	fetal bovine serum

Chapter 1. Introduction

1.1. The power of nanoparticles

Nanomaterials are defined as materials that are between 1 to 100 nanometers in size in at least one dimension and exist in a wide variety of forms and complexity. These include natural nanostructures such as wax crystals covering the leaves of the lotus flower, to the more complex bulk nanoparticles synthesized in laboratories. Materials at the nanoscale hold unique properties that are different from their counter bulk. With decreasing particle size, the surface area to volume ratio significantly increases. In addition, the high specific surface area introduces enhancements in physicochemical, electrical, optical, magnetic and quantum properties. For instance, gold nanoparticles have more reactivity than the bulk version material which is composed of the same chemistry.¹ Another well-known example are carbon nanotubes, which form highly conductive nanowires with a diameter that is only a few nanometers and a length that can extend for long distances.² Lastly, nanomaterials have dimensions and properties compatible with biomolecules, such as DNA and proteins. Thus, nanomaterials have great promise in biological applications. For example, lipid-nanoparticles, such as liposomes, are already being used clinically to deliver drugs and enhance their efficacy.³ The growing field of nanomaterials is pushing the boundaries of biotechnologies and nanomedicine.

1.2. Bioimaging at the nanoscale

Nanomaterials are being developed as tools for bioimaging. Designing suitable bioimaging probes requires multiple criteria to be taken into consideration. The size of these probes should be small enough to enter cells *via* endocytosis. Although highly unusual, some could even enter passively (see results in this thesis). To be taken up by cells efficiently, they should have high dispersibility and colloidal stability, with no aggregation or agglomeration and a polydispersity index below 0.2.⁴ In addition, nanomaterials need to have low toxicity, and good biocompatibility, meaning that they should not perturb any biological processes. And lastly, they must have chemical and photostability, meaning they must be bright and have high resistance to photobleaching and or blinking. Numerous nanotools have been developed for bioimaging applications over the years including quantum dots (QDs) and upconverting nanoparticles (UCNPs) among many others. These systems offer several benefits over conventional fluorescent imaging dyes including high

photostability, longer circulation time and the presence of different functional groups for post modification to target specific cells and/or sites within cells.⁵

QDs were developed in the 1980's and have been studied for several decades. QDs are small semiconductor particles or nanocrystals with diameters that range between 2 -10 nanometers. Their fluorescence occurs due to the quantum confinement effect, which means that they can emit light at different regions of the visible spectrum based on their particle size. The quantum confinement effect describes electrons in terms of energy levels, potential wells, valence bands, conduction bands, and electron energy band gaps and directly relates to the size of the NPs. Represented in **Fig.1**, smaller QDs have a higher quantum confinement effect, causing emission in low wavelengths (blue) due to the higher energy required to excite electrons. Larger particles require less energy and emit light with longer wavelengths (red).⁶ Although they have great optical properties, QDs are highly toxic to cells. They are often comprised of cadmium and lead, which are toxic *in vivo* and have detrimental consequences on biological processes (*i.e.* they cause an increase in reactive oxygen species).^{3,4}

UCNPs are also being developed for bioimaging applications, as they can overcome some of the limitations of QDs and can emit from the UV to the near IR region of the spectra, depending on the metal ion and its concentration. Their ability to absorb light at longer wavelengths and emit photons with shorter wavelengths is unique to these nanoparticles, and allows for biological imaging.⁹ Specifically, they absorb in the NIR region, which can more effectively penetrate tissues and cause less damage due to their low energy wavelengths. Their optical properties are ideal to avoid autofluorescence, which typically occurs in cells.¹⁰ UCNPs also have high photostability when compared to conventional dyes, however, they can lack chemical stability and/or have low quantum yields. Additionally, although unique for their optical properties UCNPs require coating (*i.e.* Oleate) to prevent aggregation in aqueous environments, which can cause toxicity in biological systems.¹¹

In addition to improving QDs and UCNPs for biological use, other nanomaterials are being explored to find alternatives. An ideal nanoparticle for bioimaging would have exceptional optical performance, high chemical and photostability, great aqueous dispersion, low cytotoxicity, and good biocompatibility.

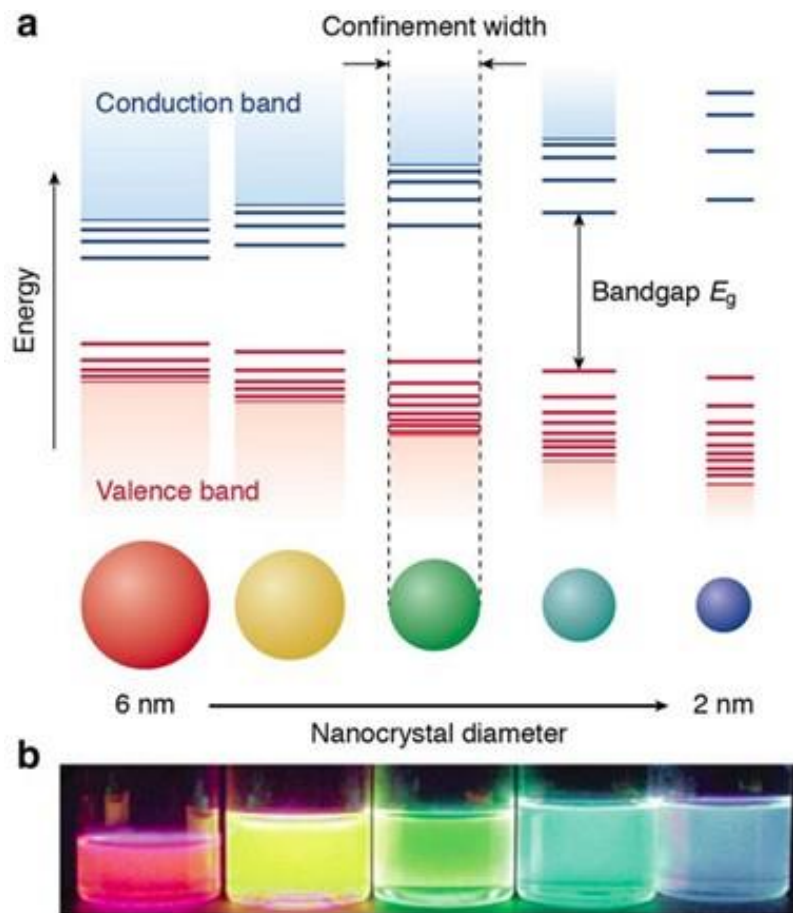


Figure 1. Quantum dots and their relative energy and fluorescence. (A) A schematic shows the quantum confinement effect: the bandgap of the semiconductor nanocrystal increases with decreasing size. The energy separation between the band-edge levels also increases with decreasing size. (B) A photograph shows five colloidal dispersions of CdSe QDs with different sizes, their excitation with UV light. The color of the photoluminescence changes from red to blue as the QD diameter is reduced from 6 to 2 nm.

Carbon-based nanomaterials are of particular interest given that their composition is highly biocompatible, and for their versatile physico-chemical and optical properties as will be described below.

1.3.Introduction to CDs

Since their discovery by Xu et al. in 2004, CDs have garnered attention over the last two decades. CDs are carbon-based nanoparticles that are quasi-spherical in shape, usually less than 10 nm in size, and are mostly composed of carbon, hydrogen, oxygen, and nitrogen. They are predominantly amorphous with a core consisting of a mixture of sp² and sp³ hybridized carbons.¹² CDs are particularly interesting due to their facile and inexpensive synthesis. They can be prepared using an array of techniques with a wide range of carbon-based materials such as orange juice, candle soot, leaves, or from simple molecules like monosaccharides, citric acid, and amino acids, like proline^{2,13-15}. The precursors chosen for the synthesis of the CDs impact their physico-chemical properties, including the functional groups that are present at their surface and optical profiles. CDs can be prepared to have tunable fluorescence in the UV, visible and near IR region of the spectrum, while offering high quantum yield ranging from 10% to 80%.¹⁶ The exact mechanism by which CDs exhibit fluorescence is not entirely understood, although contributing factors likely include the quantum confinement effect, core state, and surface states. The core is an amorphous or crystalline structure of a few nm in size, is photostable, and generally fluoresces in the blue visible light of the spectrum.¹⁷ **Fig.2** shows a schematic of the carbon core- and molecular-state fluorescence mechanism which has been suggested to be the main cause of CD fluorescence. For this mechanism, it is believed that fluorophores are formed by the precursors followed by the nucleation of the carbon core, which continues to grow through the consumption of fluorophores.¹⁸ In addition, several studies have shown that CDs can be resistant to photobleaching and blinking, which is advantageous for bioimaging compared to conventional dyes and probes which typically bleach within seconds of exposure to light.^{19,20} Furthermore, they are temperature and pH-sensitive making them excellent sensors for environmental and intracellular applications.^{21,22} Lastly and most importantly, they appear to have low cytotoxicity and good biocompatibility²³⁻²⁶. Thus, CDs meet a lot of the criteria needed for bioimaging applications, warranting further studies of CDs in more biological contexts.

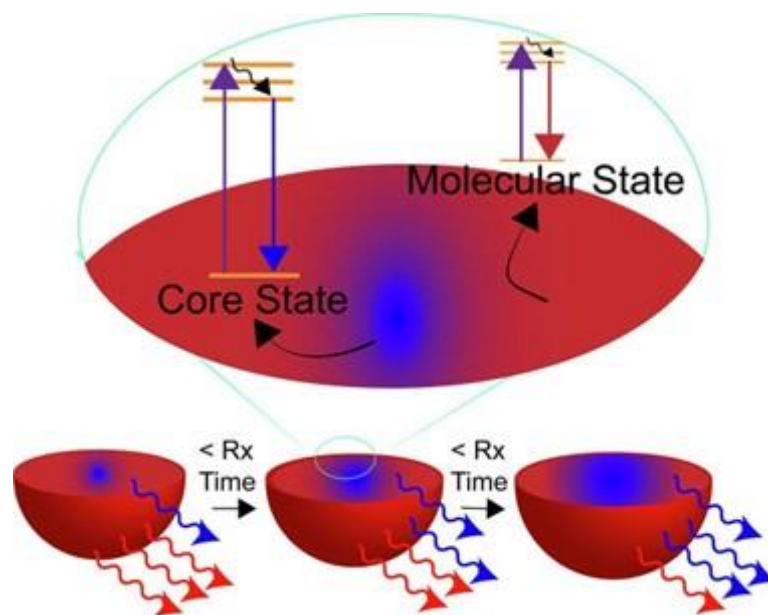


Figure 2. Graphical representation of the carbon core- and molecular-state fluorescence mechanism. As the carbonizing reaction conditions increase, fluorophores are formed by consuming the precursors, followed by the formation of the carbon core. The core increases in size through fluorophore consumption as the reaction progresses. A zoomed in portion shows the energy transfer at the core and molecular states.

1.4. CDs as bioimaging nanotools

CDs are nanoparticles with versatile optical properties. Their tunable fluorescence, low cytotoxicity and biocompatibility have made them ideal for use as bioimaging and diagnostic tools.²⁷⁻²⁹ Since biocompatibility was a high priority, CDs were shown to be safe to use in biological systems. For instance, Wang *et al.* (2017), showed that CDs have no effect on the viability of HeLa cells after treatment with concentrations up to 300 µg/mL.^{14,30} Similar results were obtained in human embryonic kidney HEK-293 cells, human hepatocellular carcinoma HepG2 cells, and human colorectal adenocarcinoma HT-29 cells.^{19,30,31} In addition, Yang *et al.* (2009) tested the toxicity of CDs *in vivo*. Mice from two groups were injected with two different dosage of CDs, 8 and 40 mg carbon core-equivalent/kg of body weight, with no significant impact on their health, including kidney function, up to 4 weeks.¹⁹ Yang *et al.* (2009) also reported that CDs compared favorably with commercialized CdSe/ZnS QDs that are currently being used for imaging applications. Both exhibit strong fluorescence properties with excitation at 440 nm. However, PEG-CdSe/ZnS QDs were found to be 50% and 25% more cytotoxic in porcine renal proximal cells and human epidermal keratinocytes, respectively, compared to functionalized PEG-CDs.¹⁹ While these results are promising, it will be crucial to carry out more *in vivo* studies on different types of CDs to determine their true potential.

CDs are also being developed to target specific organelles, where they could be used as imaging tools to reveal changes after perturbation. Indeed, Macairan *et al.* (2020) demonstrated the successful use of dual emission CDs in glioblastoma cells to sense changes in lysosomal pH in response to the administration of diclofenac and metformin, drugs typically used to treat gout and blood sugar, respectively, and are currently in clinical trials as cancer therapies.³² In another study by Macairan *et al.* (2019), dual emission CDs were used to sense precise temperature changes in cells, although they were not targeted to a specific organelle. CDs have been reported to localize outside the endomembrane system, where they could be useful for imaging other compartments and organelles.²⁷ For instance, Pan *et al.* (2015) showed that CD-treated MCF-7 cells had fluorescence throughout the entire cell, including the nucleus. This finding was quite interesting since the majority of studies using CDs for bioimaging primarily report localization in the endomembrane system.^{33,34} Therefore, different CDs could have different localization patterns and fluorescent properties depending on their physico-chemical properties and how they interact with the subcellular environment.

While there is a wealth of information describing the uptake and subcellular localization of different nanoparticles that vary in shape, size, surface charge, and functionality, very little is known about CDs. Other than toxicity, few biological studies have been performed with CDs. However, our knowledge of nanoparticles could be useful to optimize CDs. Nanoparticles are often between 2 – 100 nm in size, have surface charge, and enter cells via micropinocytosis, clathrin-dependent endocytosis, caveolae-dependent endocytosis, or other mechanisms (**Fig.3**).³⁵ Nanoparticles entering through micropinocytosis or clathrin-dependent mechanisms typically move through early and late endosomes to the lysosomes, which have low pH environments and enzymes that mediate the breakdown and degradation of biological materials. However, those entering via caveolin-mediated uptake could pass into other endomembrane systems including the ER and golgi .³⁶ Each entry mechanism is distinct and designing nanoparticles that target these could be advantageous depending on their potential use. For example, a lysosome biosensor should enter via clathrin-mediated endocytosis, while caveolin-mediated uptake could be used to avoid proteolytic degradation. The choice of pathway depends largely on their size and the functionalized groups present on their surface. For example, NPs composed of poly lactide, poly ethylene glycol and silica are internalized by clathrin-mediated endocytotic pathway, while NPs composed of other lipids enter *via* non-energy-dependent pathways as the structure of these NPs are more similar to the cell membrane.³⁷

The ideal physico-chemical properties of a nanoparticle for uptake and localization will vary depending on the cell type.³⁸ Santos *et al.* (2011) treated monitored the uptake of carboxylated polystyrene nanoparticles in 1321N1 and A549 cells. They found that 132N1 cells took up these nanoparticles mainly *via* clathrin-mediated endocytosis, while A549 cells used a caveolin-mediated pathway, suggesting that various cell types may employ different entry routes for the same nanoparticles.³⁹ In another study, Chithrani *et al.* (2006) found that gold nanoparticles (AuNPs) of 50 nm were taken up more strongly by Hela cells compared to AuNPs that were 14 or 74 nm in size.⁴⁰ In addition, Shan *et al.* (2011) found that the uptake of AuNPs in HeLa cells increased with size over a range of 4, 12 and 17 nm. The shape of nanoparticles also influences their uptake.⁴¹

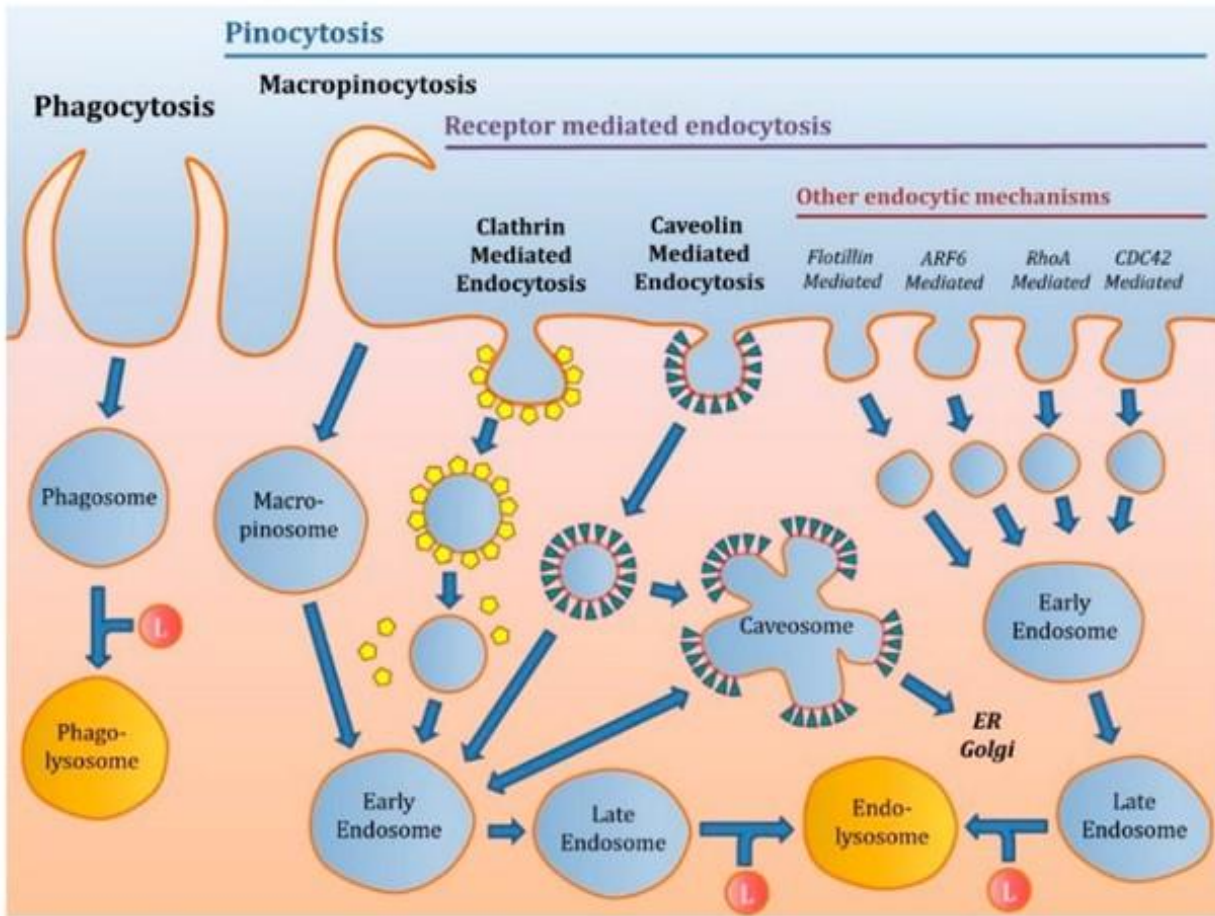


Figure 3. Uptake of nanoparticles in human cells. A cartoon schematic illustrates the main endocytic pathways for uptake of NPs in cells. Clathrin-mediated endocytosis and caveolin mediated endocytosis are the main receptor-mediated endocytosis for nanoparticle where they can traffic from endosomes to lysosomes.

Chithrani *et al.* (2006) showed that spherical AuNPs were five-fold higher in their rate of uptake compared to rod-shaped AuNPs in HeLa cells. It is important to note that they coated their AuNPs with transferrin to force their uptake by clathrin-mediated endocytosis.⁴⁰ Xu *et al.* (2008) similarly compared different layered double hydroxide nanoparticles (LDH NPs). LDH NPs are typically used as drug delivery systems for plasmid DNA, and are versatile, biocompatible and have low cytotoxicity. They found that LDH NPs that were spherical in shape were internalized more readily by clathrin-mediated endocytosis compared to rods in HEK 293T and CHO cells. However, they found that the nanorods entered the nucleus, whereas the nanospheres remained in the cytoplasm.⁴²

Making nanoparticles cationic (+ve) or anionic (-ve) can also influence their mechanism of uptake. Many phospholipids are negatively charged, favoring the uptake of positively charged nanoparticles. However, their charge could influence toxicity, for example by permeabilizing the membrane and causing cell death. Dausend *et al.* (2008) demonstrated that +vely charged nanoparticles (+NPs) were taken up at higher rate compared to -vely charged nanoparticles (-NPs). They also found that adding Dynasore to inhibit dynamin, which is required for clathrin- and caveolin- dependent endocytosis, by assembling around the neck of the vesicles to mediate their abscission upon entry, caused a decrease in both the uptake of +NPs and -NPs, but had a stronger impact on +NPs. When chlorpromazine was used to inhibit clathrin-dependent pathways, only +NPs were inhibited from entering the cells. Thus, multiple pathways could be used by nanoparticles for their uptake, which depends on their surface charge.⁴³

Surface chemical modification or functionalization of nanoparticles is often required to decrease toxicity, increase stability and to control cellular uptake, as outlined above. Surface functionalization includes adding PEG, a negatively charged carboxyl (-COOH) group, a neutral hydroxyl (-OH) group, or a positively charged amine (-NH₂) group.³⁷ Tao *et al.* (2016) reported that polydopamine functionalization enhanced nanoparticle uptake in breast cancer cell.⁴⁴ Jiang *et al.* (2010) compared the uptake of polystyrene NPs and amino functionalized polystyrene nanoparticles (NPS-NPs). NPS-NPs were rapidly internalized by mesenchymal stem cells at a higher rate compared to non-modified nanoparticles, and entered using a clathrin-mediated mechanism of uptake.⁴⁵ This highlights the importance of surface chemical modifications for cellular interactions and efficiency of uptake.

1.5. Addressing the Gap

CDs have the potential to be suitable bioimaging tools due to their ideal properties. Despite this, there remains a significant knowledge gap in our understanding of their behavior in live cells. CDs have been widely researched in a plethora of different applications such as bioimaging, drug delivery and light therapy owing to their optical properties, high quantum yield and versatile surface chemistry. However, few studies demonstrate how CDs localize in different cell types, and how functionalization affects their uptake and localization. Although a large amount of knowledge is available about the cellular entry of nanoparticles in cells in general, very few have studied CDs in this context. Understanding the mechanism of entry and differences in localization of different CDs in different cell types can improve our knowledge of how to use CDs for biological applications.

1.6. Objectives

The goal of this work was to synthesize and characterize five different amine passivated CDs with increasing nitrogen content *in vitro* and in two different human cell types.

Objective 1. Determine how using different amine passivating agents impacts the physicochemical and optical characteristics of CDs. Methods to measure physicochemical characteristics include using TEM to measure size and morphology, FT-IR and XPS spectroscopies to study the surface composition, and zeta-potential to measure surface charge. Methods to measure optical properties include UV-Vis absorbance, fluorescence spectroscopy and quantum yield.

Objective 2. Determine how different properties of CDs impact their uptake, toxicity and localization in different cultured human cells. Methods include using fluorescence microscopy with live cells after treatment with different concentrations of CDs to measure uptake and localization, metabolic assays to measure toxicity, and co-localization studies using lysotracker dye to visualize the lysosomes.

Chapter 2. Materials and Methods

2.1. Chemicals and reagents

Citric acid, ethylene-diamine (ED2), diethyltriamine (DT3), tetraethylenetriamine (TT4), tetraethylenepentamine (TP5), pentaethylenehexamine (PH6), acetone and ethanol were purchased from Sigma Aldrich. Milli-Q water was produced in-house. Phosphate buffer solution (PBS, 1X) and Dulbecco's modified Eagle medium (DMEM) were purchased from Wisent. HyClone™ Calf Serum and LysoTracker™ Red DND-99 were purchased from Thermo Scientific. The WST-8 Cell Proliferation Assay Kit was purchased from Cayman Chemical. All reagents were of analytical grade and were used as is, without the need for further purification.

2.2. Synthesis of carbon dots

All CD's were synthesized using a CEM Discover SP microwave reactor. For all CD's synthesis, 0.384 g (500 mM) of citric acid were added to 4 mL of distilled water and 375 mM of amine passivating agent in microwave reaction tube. The amine passivating agents used were ethylene-diamine (ED2), diethyltriamine (DT3), tetraethylenetriamine (TT4), tetraethylenepentamine (TP5), pentaethylenehexamine (PH6). The reaction solutions were sonicated for 15 minutes, or until a homogenous solution was observable. It was heated to 210 °C for a period of 10 minutes. After the completion of the reaction, the samples were dialyzed in Milli-Q water using a cellulose dialysis membrane (molecular weight cut-off = 3.5-5.0 kDa) to remove unreactive and unwanted materials. The samples were dialyzed for a period of 5 days, where visible decrease in color was observable due to the loss of unwanted product. To improve the dialysis process, the water was changed twice a day. The samples were then purified by washing twice with acetone and twice with ethanol. After each wash, the precipitate was collected by centrifugation at 10 000 x for 10 minutes and the supernatant discarded. The resulting materials were left to dry for a period of 12 to 24 hours in an oven at 80 °C. The final dried product was crushed into a fine powder and resuspend in nano-pure water. Finally, for biological purposes and to prevent contamination, the resuspended materials were filtered through a 0.22 µm nylon filter.

2.3. Fluorescence spectroscopy

Fluorescence spectra of aqueous CD's were collected using a Cary Ellipse Fluorescence Spectrophotometer (Agilent Technologies) using a 1 cm quartz cuvette. Prior to the analysis the CD's concentration was adjusted to an absorbance value of 0.1 a.u. to avoid potential inner filter

effects. All fluorescence data were collected by setting λ_{ex} at 350nm with a range of 200 to 800nm (1nm intervals). The excitation and emission slits were set to a width of 5 nm with a PMT voltage at 600 V and a scan rate of 600nm/min. All data were processed using Cary Eclipse software. The spectra were background corrected for the solvent (Milli-Q water).

2.4.UV-vis Absorbance Spectroscopy

Absorbance spectra was acquired using a Cary 5000 series UV-Vis-NIR Spectrophotometer (Agilent Technologies). The UV-visible absorption spectra were collected over a range of 200-800 nm using a 1 cm quartz cuvette. A resolution of 1 nm and a bandwidth of 2 nm were set with a scan speed of 600 nm s⁻¹ and wavelength changeover at 350 nm were used for analysis. Data were processed using Cary Eclipse software. The spectra were background corrected for the solvent (Milli-Q water).

2.5.Fourier Transform Infrared Spectroscopy

FTIR spectra were collected using a Thermo Scientific Nicolet iS5 equipped with an iD5 ATR accessory. An approximately of 10 μ g of sample was used for the analysis. The spectra were collected using 64 scans with a resolution of 0.4 cm⁻¹, a gain of 1, an optical velocity 0.4747, and an aperture setting of 100. Data was processed using the Omnic 9 software.

2.6. Transmission Electron Microscopy

TEM grids (3 mm, 200 mesh Lacey/carbon-coated copper grid) were prepared by pipetting a 2 μ g/mL dispersion of each CDs onto the surface followed by evaporation of isopropanol solvent. The TEM images were collected using the Talos microscope operating at 120 kV. The images were processed, and the carbon dot sizes were measured using the Fiji imaging software.

2.7.Quantum Yield

Quantum yield values were acquired on a PTI QuantaMaster 8075 spectrofluorometer (Horiba) equipped with a 75 W Xenon lamp and a Czerny-Turner monochromator and an integrating sphere (K-Sphere Petit, Horiba). All quantum yields measurements were done in milli-Q water in a 1 cm quartz cuvette, the excitation and emission slits were set to a width of 5 nm, and the excitation was set to 350 nm; the spectra from 3000-800 nm were collected. The quantum yields of the blue component were collected from 300-550 nm. Scans were done in triplicate with dwell time of 0.25 sec. Data were processed using the FelixGX software.

2.8. Zeta-Potential

Zeta-potential measurements were acquired on a Malvern Zetasizer Nano ZSP using colloidal dispersion of each amine passivated CDs (Ed2-, DT3-, TT4-, TP5- and PH6-CDs) at a final concentration of 10 µg/mL in milli-Q water. Zeta-potential values are reported as the average of 3 independent batches of each CDs.

2.9. Photobleaching of CDs

Aqueous dispersions of ED2-, DT3-, TT4-, TP5-, and PH6- passivated CDs were prepared at final concentration of 10 µg/mL in 40 mL volumes. Each dispersion was placed under a 15 W UV lamp for 0, 0.33, 0.5, 0.66, 1, 2, 3, 6, and 12 hours using a UVP Chromato-VUE® C-70G viewing cabinet. At every timepoint, an aliquot was removed to record its respective fluorescence intensity. The remaining percent fluorescence was calculated with the following equation.

$$\text{Remaining Fluorescent \%} = \frac{\text{Fluorescent intensity at } x \text{ point time } (\lambda_{ex} = 350\text{nm})}{\text{Fluorescent intensity at time point 0 } (\lambda_{ex} = 350\text{nm})}$$

2.10. Cell Culture

HFF-1 (Human foreskin fibroblast) and HeLa (human cervix adenocarcinoma) cells were cultured in Dulbecco's modified Eagle medium (DMEM; Wisent) supplemented with 10% (v/v) fetal bovine serum (FBS; Wisent) and 2 nM L-Glutamine (Wisent). Cells were maintained in a humidified incubator set to 37°C with 5% CO₂ and passaged at 75-100% confluency or as needed for the analysis of CDs in cells. Cells were trypsinized for plating by adding 500 µL of trypsin to the dish. After, the dish was placed in the incubator for 10 minutes to allow the cells to detach. HeLa cells were resuspended in 10 mL of pre-warmed DMEM (10% FBS) media and thoroughly mixed before transferring 1 mL to a new dish containing 10 mL of pre-warmed media. HFF-1 cells were resuspended in 7 mL of pre-warmed DMEM (10% FBS) media and 3 mL was transferred to the new dish containing 10 mL.

To measure the uptake of CDs in cells, they were plated in a 12-well glass bottom dish (CellVis) at a confluency of 30-40% for HeLa and 50%-60% for HFF-1 and left to adhere. The cells were then treated with 100 µL of each CDs that were adjusted to the same optical density over 24 hours to assess their fluorescence intensity in cells (ED2, DT3, PH6 at 1000 µg/mL, TT4 at 750 µg/mL and TP5 at 600 µg/mL). Prior to imaging, the cells were washed with 1X PBS (phosphate-buffered saline) and replaced with fresh, pre-warmed media.

To monitor where CDs localize in cells, they were plated on individual 35 mm glass bottom dish (CellVis) at 30-40% confluency for HeLa and 50%-60% HFF-1 and left to adhere before being treated with 1000 µg/mL of CDs for 24 hours. To image the lysosomes, LysoTracker™ DND-99 was added to treated cells at a final concentration of 75 nM and left in the incubator for 45 minutes before imaging. Prior to imaging, the cells were washed with 1X PBS (phosphate-buffered saline) and replaced with fresh, pre-warmed media.

2.11. Cytotoxicity

HFF-1 and HeLa cells were plated in 96-well dishes at 4,000 – 5,000 cells per well and left to adhere for 24 hr. Then, cells were treated with increasing concentrations of each CDs (0 to 10 000 µg/mL⁻¹) for three generation times (72 hr and 108 hr for HeLa and HFF-1 cells, respectively). Cytotoxicity was assessed using the WST-8 cell proliferation assay (Cayman Chemical) as per manufacturer's instructions. For each well, 10 uL of reagent was added for 4 hours, then the optical density (OD) values were obtained using the TECAN 200 PRO plate reader at a wavelength of 490 nm. Cell viability was measured as a ratio of the signal of treated cells *vs.* control (untreated cells):

$$\%cell\ viability = \frac{OD(490\ nm)_{sample}}{OD(490\ nm)_{control}} \times 100\%$$

All measurements were repeated in triplicates and the means were plotted with standard deviation using PRISM software. The IC50 was obtained by measuring the concentration at which half the population (50%) remained alive with the CDs treatment. HeLa and HFF-1 cells were imaged using a NIKON brightfield microscope to ensure that they were plated with the appropriate confluency, and to ensure that changes in density were not caused by contamination or other unrelated issues.

2.12. Microscopy

Cells were imaged using the Nikon-TIE inverted epifluorescence microscope with a Lambda XL Xenon light source using a 60x Plan Apo objective lens (NA1.4) or a 100x S Fluor objective lens (NA 1.3), a Piezo Z stage (ASI), a Photometrics Evolve 512 EMCCD camera and Elements 4.0 acquisition software (Nikon). Excitation at 380 nm was used to capture fluorescence at 450 nm using a 400-600 nm bandpass (Chroma CT500/200bp) filter.

2.13. Statistical Analysis

To assess the cellular uptake of CDs, background intensities were subtracted by using the threshold tool and a fixed value was set for all images when comparing mean intensity within the same cell type. The mean intensity values were then plotted on a whisker box plot and a one-way ANOVA was performed along with a post-hoc paired t-test.

To assess the co-localization of CDs in the lysosomes, images were first deconvolved using AutoQuant X software. These images were then processed using the Biop Jacop plugin available in Fiji to calculate their Pearson's correlation. The values (% correlation) were then plotted on whisker box plot and a one-way ANOVA was performed along with a post-hoc paired t-test.

Lastly, to assess the presence of CDs in the cytosol, the background intensity was subtracted from the cytosol intensity, then the mean intensity signal was determined from three regions of interest in the cytosol. Each measurement was performed in triplicates. The mean intensity values were then plotted on a whisker box plot and a one-way ANOVA was performed along with a post-hoc paired t-test.

Chapter 3. Results

3.1. Optical properties of amine-passivated CDs

Due to their optical properties, carbon dots (CDs) have the potential to be used as imaging tools for diagnostics or drug discovery. We determined how functionalizing carbon dots (CDs) with different amine passivating agents affects their physicochemical properties and cellular uptake. CDs were synthesized *via* a microwave-mediated reaction with 500 mM of citric acid and 375 mM of different passivating agents as described in the materials and methods. We chose these agents (ethylenediamine (ED2), diethyltriamine (DT3), tetraethylenetriamine (TT4), tetraethylenepentamine (TP5) and pentaethylenehexamine (PH6)) because they have different amine chain lengths, which could confer different physicochemical properties such as surface functional groups, surface charge, shape, and size, which could affect their uptake in cells.

The optical properties of the different amine-passivated CDs were characterized using absorption and fluorescence spectroscopy. Absorbance spectroscopy was used to measure the spectra of the CDs at concentrations of 10 $\mu\text{g/mL}$. As shown in **Fig. 4A** there were two main absorption bands centered at 240 nm and 350 nm, which reflect the $\pi \rightarrow \pi^*$ transition of the aromatic sp^2 domains and the $n \rightarrow \pi^*$ transition of the C=O bond or amine functional groups, respectively. We also measured the fluorescence properties of the CDs when dispersed in aqueous solution at a concentration of 10 $\mu\text{g/mL}$. As shown in **Fig. 4B**, following excitation at $\lambda_{max} = 350$ nm, the spectra of each of the different CDs show fluorescence at 450 nm. Finally, to determine the fluorescence efficiency of the different CDs, the quantum yield was measured using an integrating sphere and determined to be 15%, 25%, 10%, 22% and 20% for ED2, DT3, TT4, TP5 and PH6-passivated CDs, respectively (**Fig. 4C**). Although there was no observable trend, a high quantum yield can be explained by the increased passivation which reduces the number of non-radiative traps. There is no increased benefit beyond DT3.

3.2. Physicochemical properties of amine-passivated CDs

We determined the physicochemical properties of the different amine-passivated CDs. To evaluate the chemical groups on their surface, Fourier transform infrared spectroscopy (FTIR) was used. The FTIR results in **Fig. 5A** showed similar spectra for each of the CDs, with the presence of a broad carbonyl signal from 1614 to 1753 cm^{-1} attributed to the presence of the carboxylic acid (C=O).

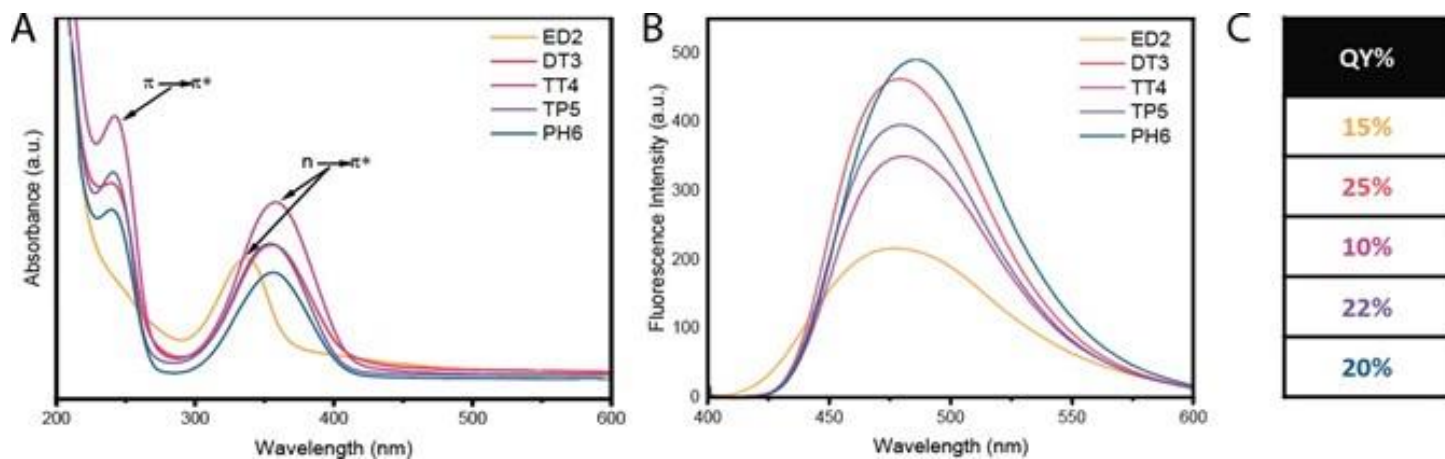


Figure 4. Optical properties of amine-passivated CDs. (A) A graph shows the absorption (a.u.) of CDs in aqueous solution at various wavelengths. Absorption peaks are visible at 240 nm and 335–355 nm, which reflect the $\pi \rightarrow \pi^*$ and $n \rightarrow \pi^*$ transition, respectively. (B) A graph shows the fluorescence intensity (a.u.) of CDs in aqueous solution at various wavelengths, revealing excitation λ_{max} at 350 nm and emission λ_{max} at 450 nm. (C) A table shows the quantum yield for the different CDs as indicated (ED2, yellow; DT3, pink; TT4, magenta; TP5, purple; PH6, blue).

In addition, sp^3 C–H peaks were observed at 2964 cm^{-1} along with sp^2 C–H peaks observed near the 2830 cm^{-1} region. Lastly, amide C=O, C=C/C=N, and amine N-H/C-N peaks appeared at 1646 cm^{-1} , 1536 cm^{-1} and 1354 cm^{-1} . Although very similar, the most notable change is the progressive reduction in the carboxylic acid signal with the increase in passivation, which corresponded with an increase in the C=C/C=N and N-H/C-N peaks. The elemental composition of the CDs was then investigated using XPS analysis. The spectra for the CDs revealed three principal binding energies attributed to C1s, N1s and O1s at 280, 400 and 530 eV, respectively. Deconvolution of the C1s peak showed three main peaks with binding energies at 285, 286 and 288 eV, attributed to C-C, C-O and carboxylic C=O groups, respectively. Deconvolution of the N1s peak revealed two main peaks with binding energies at 399 and 400 eV caused by amine N-C and amide N-O, respectively. Lastly, the deconvolution of the O1s peak revealed two main peaks with binding energies at 531 and 532 eV due to the carboxyl C=O and carbonyl C-O groups. Thus, the XPS analysis agreed with the FTIR analysis (**Appendix 1**).

We extended our investigation of the surface composition of the amine-passivated CDs. **Fig. 5B** shows the XPS elemental analysis where we can see that the nitrogen content increased with higher amounts of amine in the passivating agents for ED2-CDs and DT3-CDs, but a sudden decrease was observed for TT4-CDs, TP5-CDs and PH6-CDs. To investigate the reason for these results, a more precise elemental composition analysis was performed to determine the N-O sp^2 amide and N-C/C-N sp^3 amine content. This analysis revealed a decrease in amides and increase in amines for ED2-, DT3- and TT4-passivated CDs. (**Fig. 5C**) Additionally, there was an increase in amides and a decrease in amines for TP5- and PH6-passivated CDs. This can be explained by the molecular structure of the precursors. During the synthesis, the amine passivating agents may react with the citric acid precursor and form heterocyclic intermediates, which can then crosslink and polymerize. With TP5 and PH6 agents, their long carbon-nitrogen chains can easily form 5 or 6-membered carbon rings when reacting with citric acid. They are then incorporated into the core of the CDs explaining the increase in sp^2 amine and the concomitant decrease of the sp^3 amine composition for these two CDs.

Next, the surface charges of the different CDs were measured since this property could impact their cellular uptake. The zeta potential of the CDs was measured after dispersing them in an aqueous dispersion to a final concentration of $10\text{ }\mu\text{g/mL}$.

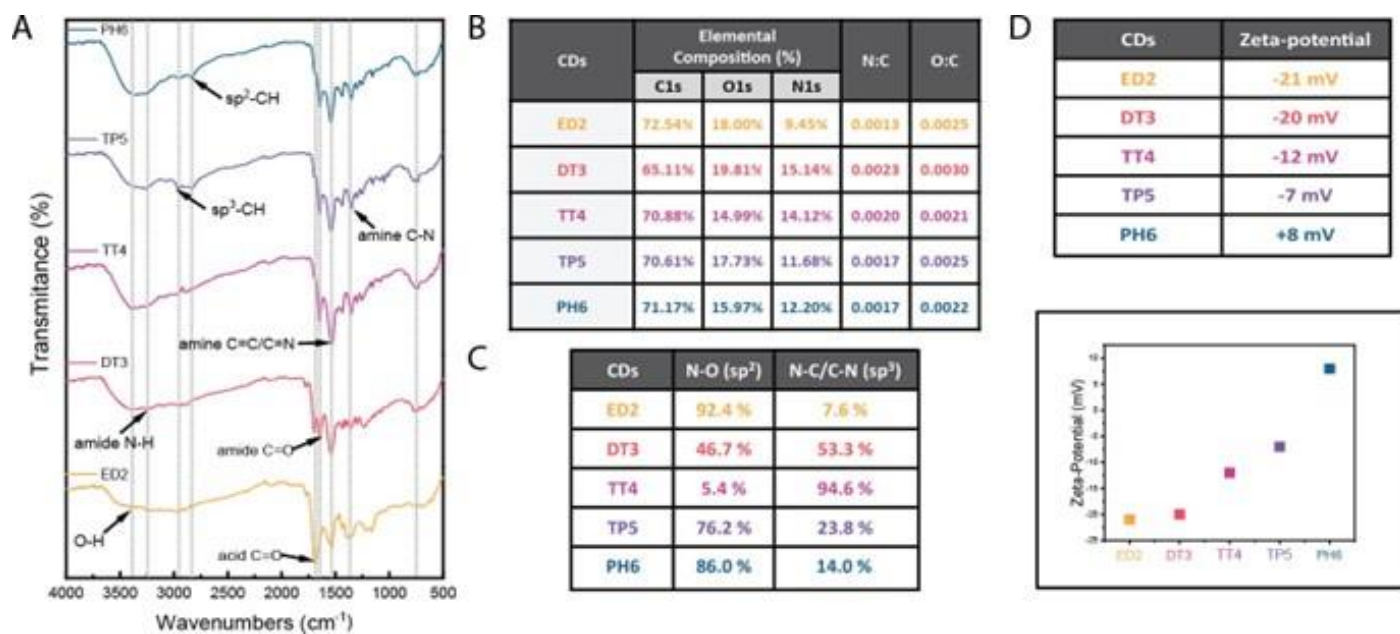


Figure 5. The surface composition and charge of amine-passivated CDs changes correlates with the amine context of the passivating agent. (A) A graph shows the stacked FT-IR spectra for each of the amine-passivated CDs. The broad carbonyl signal from 1614 to 1753 cm^{-1} indicates carboxylic acid (C=O), and sp^3 and sp^2 C-H peaks are at 2964 cm^{-1} and 2830 cm^{-1} respectively. Lastly, amide C=O, C=C/C=N, and N-H/C-N peaks appears at 1646 cm^{-1} , 1536 cm^{-1} and 1354 cm^{-1} . (B) A table shows the elemental composition determined by XPS for the N:C and O:C ratios. (C) A table shows the N-O (sp^2) vs N-C/C-N (sp^3) composition for each CD. (D) A table (top) and graph (bottom) show the zeta-potential for the different CDs, as an indication of surface charge.

As shown in **Fig. 5D**, their surface charges were measured to be -21mv, -20mv, -12mv, -7mv and +8mv for ED2, DT3, TT4, TP5 and PH6, respectively. This almost linear increase in positive surface charge correlates with the increase in amine passivation of the CDs.

Furthermore, the size and morphology of the different amine-passivated CDs were assessed as these parameters can also influence their uptake by cells. The TEM images in **Fig. 6** revealed that the CDs are quasi-spherical with sizes of 1.40 ± 0.21 nm, 2.74 ± 0.46 nm, 1.58 ± 0.47 nm, 2.00 ± 0.37 nm and 1.29 ± 0.34 nm for the ED2-, DT3-, TT4-, TP5- and PH6-passivated CDs, respectively. The size measurements for each of the CDs were spread over a Gaussian distribution ranging from 0 to 4.5 nm. In addition, their respective polydispersity indexes (PDIs) varied from 0.02 to 0.07. These PDI values are deemed acceptable for use in biological applications, as it suggests that the CDs do not aggregate

Lastly, the photostability of the amine passivated CDs in aqueous solution was assessed upon exposure to 365 nm UV light for 0, 0.33, 0.5, 0.66, 1, 2, 3, 6 and 12 hours. The graph in **Fig.7** shows how the CDs were generally resistant to photobleaching, as demonstrated by the % fluorescence remaining after different lengths of exposure to UV light. While DT3-CDs had the least resistance, PH6-CDs were the most resistant with 40.1% signal remaining after 12 hours, followed by ED2-, TT4-, TP5 and lastly DT3-CDs with 30.2%, 30.1%, 29.3% and 6.6% remaining, respectively. These data suggest that the ability of these CDs to resist photobleaching could make them ideal for use in fluorescence imaging.

3.3. Cytotoxicity of amine-passivated CDs

The chemical composition of CDs predicts that they would have low cellular toxicity. To assess this, the cytotoxicity of the different amine-passivated CDs was measured over a large range of concentrations. We tested the CDs in both HeLa and HFF-1 cells because HeLa, which are epithelial and cancerous in origin, are a common cell type used for biological studies, while HFF-1 cells are fibroblasts that are non-cancerous and are found in connective tissue. Testing different cell types is important, as their different genetic backgrounds could influence how they respond to CDs.

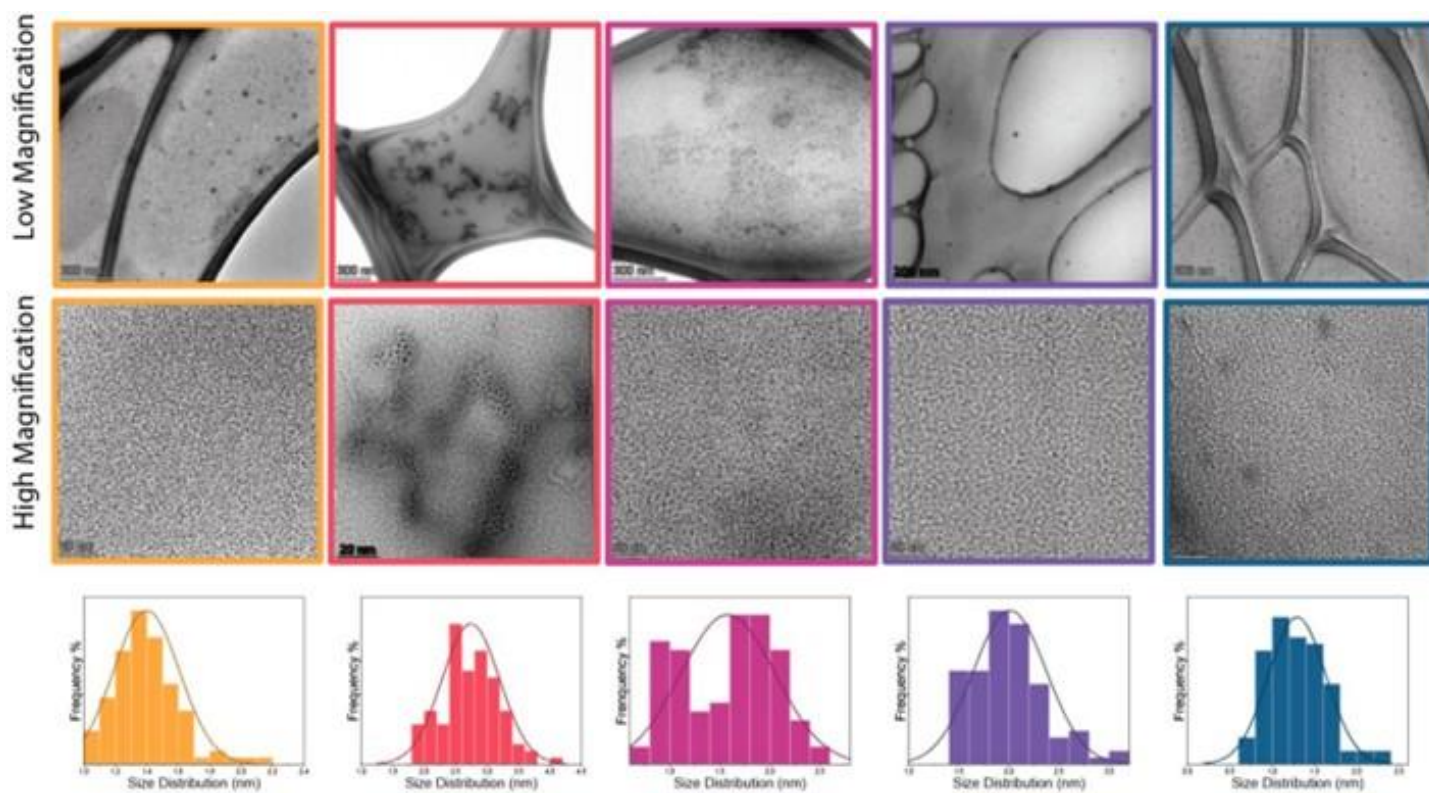


Figure 6. CDs are quasi-spherical and are close to 2nm in size. TEM images show aqueous dispersions of the different amine-passivated CDs as indicated. The CDs are quasi-spherical with sizes of 1.40 ± 0.21 nm, 2.74 ± 0.46 nm, 1.58 ± 0.47 nm, 2.00 ± 0.37 nm and 1.29 ± 0.34 nm for the ED2-, DT3-, TT4-, TP5- and PH6-passivated CDs, respectively. The size measurements for each of the CDs were spread over a Gaussian distribution ranging from 0 to 4.5 nm.

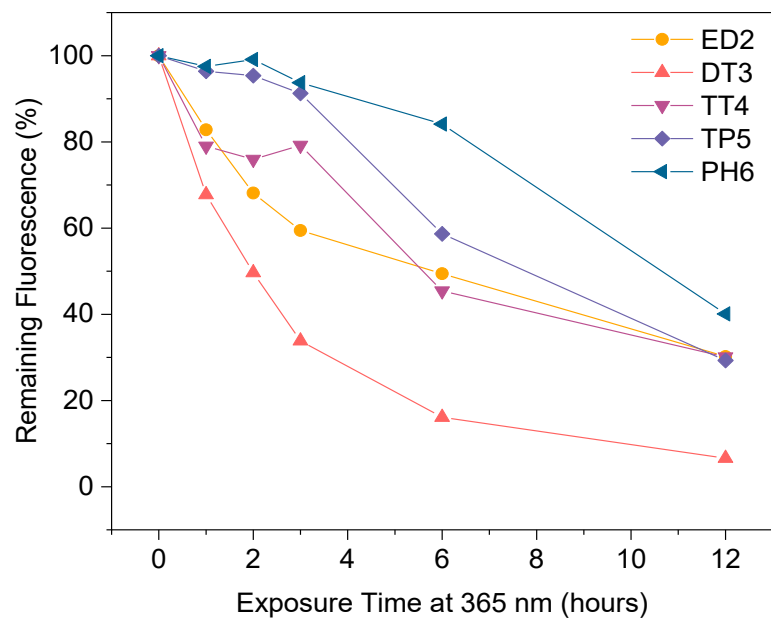


Figure 7. Amine-passivated CDs are highly photostable. A graph shows the fluorescence (%) of CDs after exposure to 365 nm light over time as indicated.

After adding varying concentrations of the different CDs to the cells and leaving them for three division cycles (72 hours for HeLa and 108 hours for HFF-1), the number of cells was measured using the WST-8 assay, which produces a colorimetric output that is proportional to the metabolic activity of cells. As shown in **Fig. 8A** and **Fig. 8B**, there was no measurable IC_{50} for toxicity (e.g., >10,000 ug/mL), or it was very high for the different amine-passivated CDs in both cell types (ED2 was 10,000 ug/mL in HeLa and HFF-1 cells, while TP5 was 7,500 ug/mL in HFF-1 cells). Therefore, as predicted based on their elemental composition, the amine-passivated CDs have little to no cytotoxicity effect on HeLa and HFF-1 cells.

3.4. Cellular uptake of amine-passivated CDs

Next, we determined how passivation impacts the uptake of the different CDs in HeLa and HFF-1 cells. Since their size and surface composition are relatively similar, the main physicochemical property that could impact their uptake is charge, which ranges from more negative (e.g., ED2-passivated CDs) to more positive (e.g., PH6-passivated CDs). To do this, HeLa and HFF-1 cells were treated for 24 hours with the different amine-passivated CDs that were adjusted to the same optical density rather than to concentration, to avoid concentration-dependent fluorescence as shown in (**Fig. 9A**). Live cells were imaged using widefield epifluorescence. As shown in **Fig. 9B** and **Fig. 9C**, each of the different amine-passivated CDs entered HeLa and HFF-1 cells, which was measured by the mean fluorescence intensity. In both cell types, there was a significant difference in the mean intensity between the CDs treatment after performing a one-way ANOVA analysis. Because significant differences were found between the mean intensities in both HFF-1 and HeLa cells, a post-hoc analysis using a paired-t test was performed to compare the intensity of PH6-CDs to the other CDs. Indeed, the PH6-CDs were significantly higher than all other CDs, suggesting that either more PH6-CDs were taken up by cells, and/or they aggregated causing brighter fluorescence due to their localization (**Appendix, Table 1**).

3.5. Subcellular localization of amine-passivated CDs

The localization of the different amine-passivated CDs was then assessed in HeLa and HFF-1 cells. Previous studies of various nanoparticles showed that they enter cells through clathrin- or caveolin-dependent endocytosis, or micropinocytosis depending on their physicochemical properties.

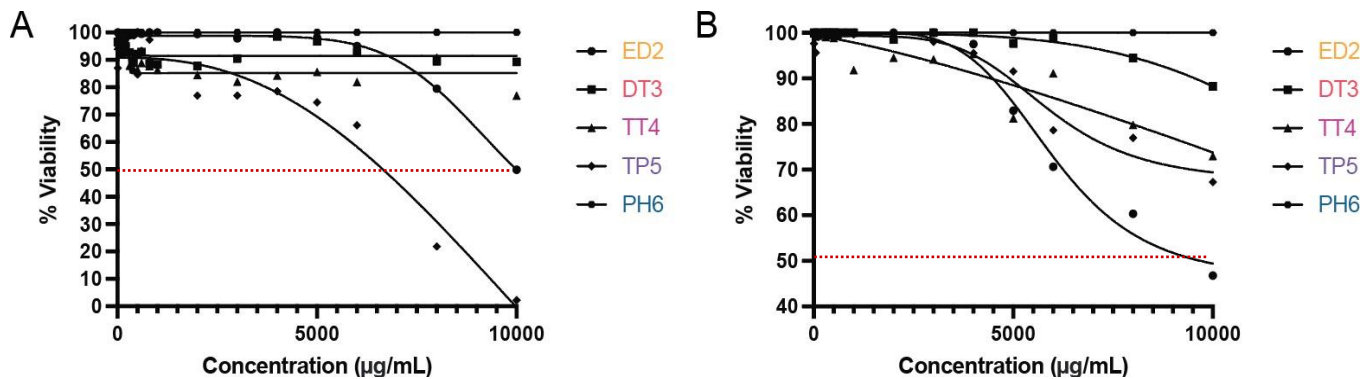


Figure 8. CDs are not highly toxic in HFF-1 or HeLa cells. (A) A graph shows the IC₅₀ (dotted line) for HFF-1 cell viability, after treatment with varying concentrations of the different CDs for three population doubling times (7,500 µg/mL and 10,000 µg/mL for TP5-CDs and ED2-CDs respectively, and >10,000 µg/mL for TT4-, DT3-, PH6-CDs). (B) An graph shows the IC₅₀ (dotted line) for HeLa cell viability, after treatment with various concentrations of the different CDs for three population doubling times (10,000 µg/mL for ED2-CDs and >10,000 µg/mL for DT3-, TT4-, TP5- and PH6-CDs)

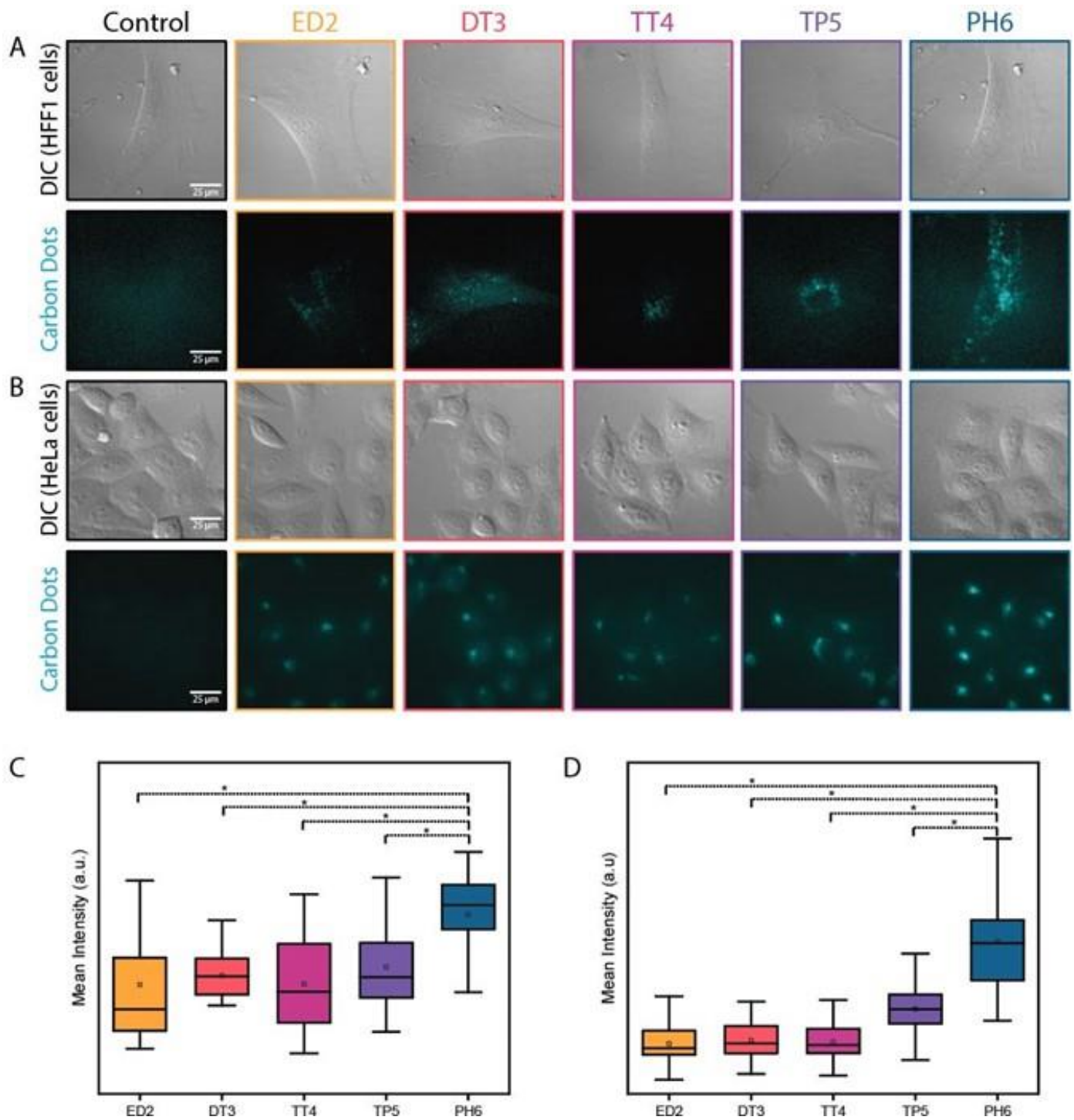


Figure 9. Cellular uptake of CDs in HFF-1 and HeLa cells. (A) Brightfield (top) and fluorescence images (bottom) of HFF-1 cells 24 hours after treatment with the CDs (blue) as indicated. Scale bar is 25 μ m. (B) Brightfield (top) and fluorescence images (bottom) of HeLa cells 24 hours after treatment with the CDs (blue) as indicated. Scale bar is 25 μ m. (C) A box and whiskers plot show the mean intensity (a.u.) of the different CDs as indicated in HFF-1 cells. Bars indicate standard deviation. One-way ANOVA and Paired t-tests to PH6 were done to show significance ($*p < 0.001$). (D) A box and whiskers plot shows the mean intensity (a.u.) the different CDs as indicated in HeLa cells. Bars indicate standard deviation. One-way ANOVA and paired t-tests to PH6 were done to show significance ($*p < 0.001$).

Regardless of these routes of entry, nanoparticles are typically trafficked through endosomes to the lysosomes. However, there could be differences in how CDs enter and localize in HeLa and HFF-1 cells. To measure this, cells were treated with the different amine-passivated CDs for 24 hours at a final concentration of 1000 $\mu\text{g/mL}$, then lysotracker dye was added 45 minutes before imaging to visualize the lysosomes (**Fig. 10A** and **Fig. 11A**). Epifluorescence microscopy was performed with live cells, and images were quantified for the extent of co-localization between the CDs and lysosome signal. A plug-in for Image J was used to calculate the Pearson's correlation coefficient, which revealed significant differences in the localization of CDs to the lysosomes. Specifically, the proportion of the different CDs that localized to the lysosomes in HFF-1 cells was 12%, 22%, 36%, 45% and 52% for ED2, DT3, TT4, TP5 and PH6-CDs, respectively (**Fig. 10B**). In HeLa cells, the proportion of CDs that localized to lysosomes was 21%, 21%, 31%, 49% and 80% for ED2, DT3, TT4, TP5 and PH6-CDs, respectively (**Fig 11B**). After performing a paired t-test, PH6-CDs significantly localized more to the lysosomes compared to the other CDs in both cell lines, suggesting that more of these dots enter the endocytic pathway, and/or are taken up in similar quantities, but are the brightest (**Appendix, Tables 2 and 3**). There was also a significant increase in DT3-CDs in the cytosol of HFF-1 and HeLa cells compared to the other amine-passivated CDs. Indeed, as shown in **Fig. 10C** and **Fig. 11C**, the average mean fluorescence intensity for selected regions of interest in the cytosol revealed that DT3-CDs were significantly higher compared to the other amine-passivated CDs in both cell lines (**Appendix, Tables 2 and 3**). This ability of DT3-CDs to localize to the cytosol could be advantageous for some imaging and nanomedicine applications.

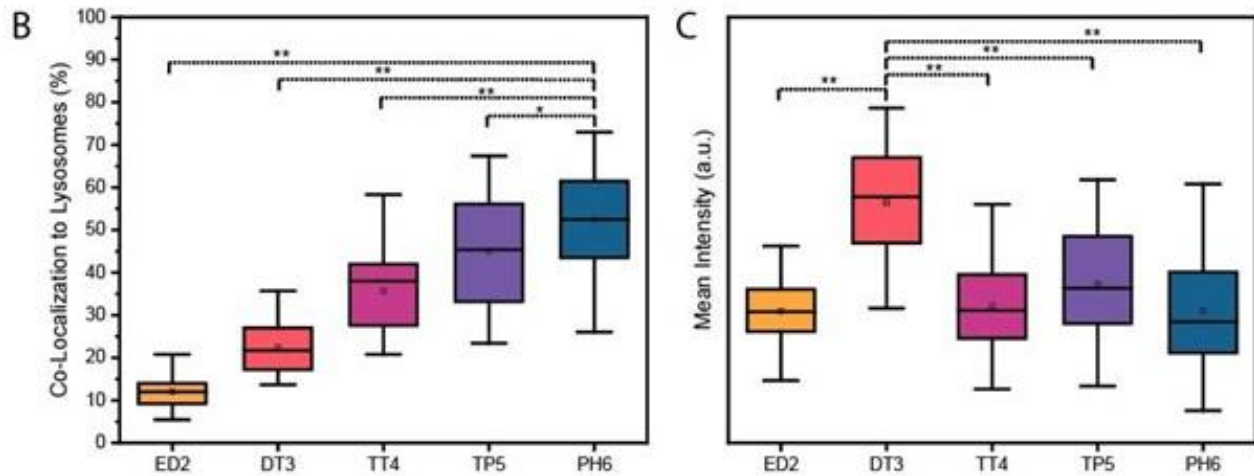
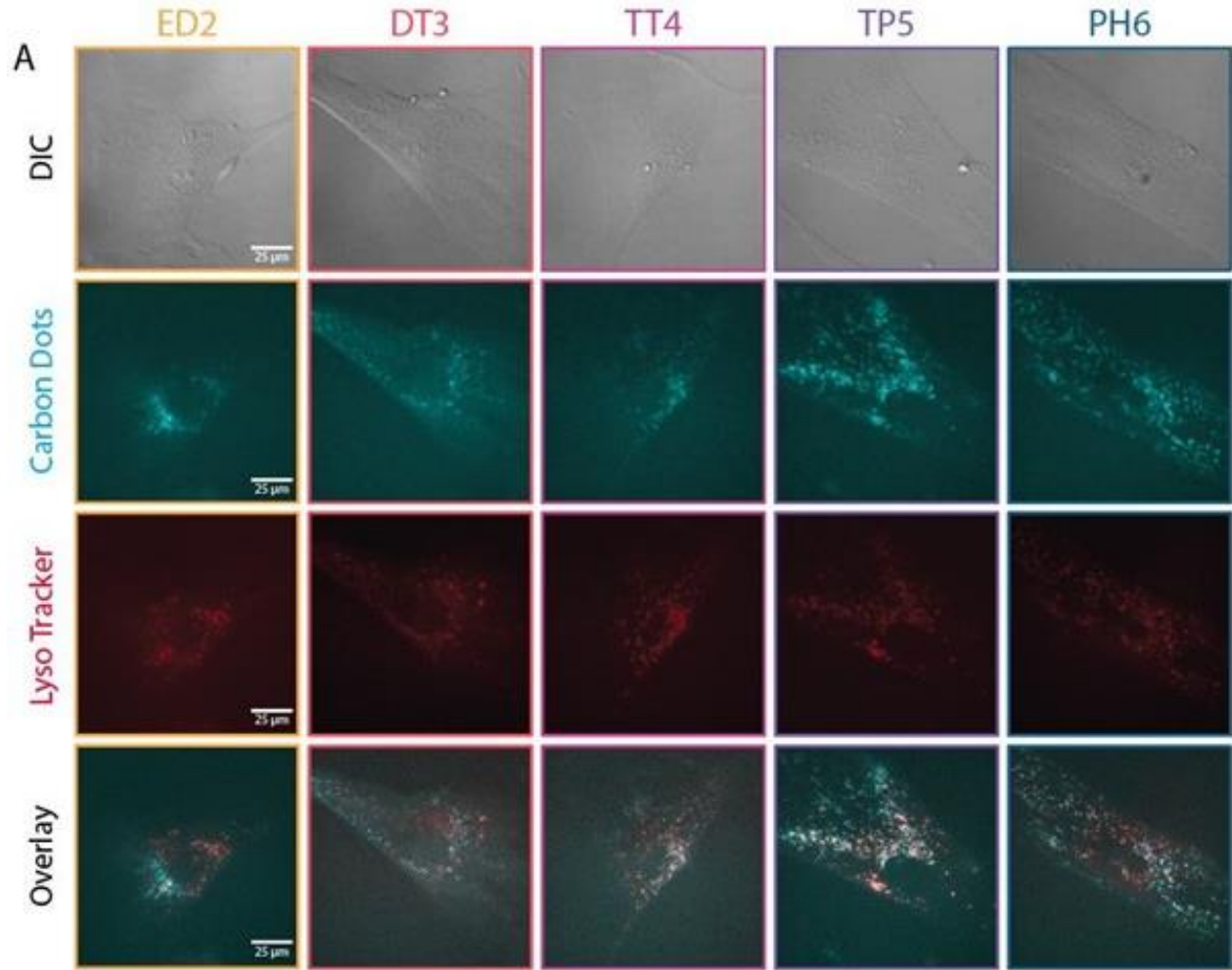


Figure 10. CDs localize to the lysosomes and cytosol in HFF-1 cells. (A) Brightfield (top) and fluorescence images show live HFF-1 cells 24 hours after treatment with 1000 µg/mL of the CDs (blue) as indicated, co-stained for lysotracker (red). The scale bar is 25 µm. (B) A box and whiskers graph show the % co-localization of CDs as indicated with lysotracker using Pearson's correlation. Bars indicate standard deviation. One-way ANOVA and paired t-tests to PH6 were done to show significance (* $p < 0.05$; ** $p < 0.001$). (C) A box and whiskers graph shows the mean intensity (a.u.) of CDs in the cytosol. Bars indicate standard deviation. A one-way ANOVA and paired t-tests to DT3 were done to show significance (** $p < 0.001$).

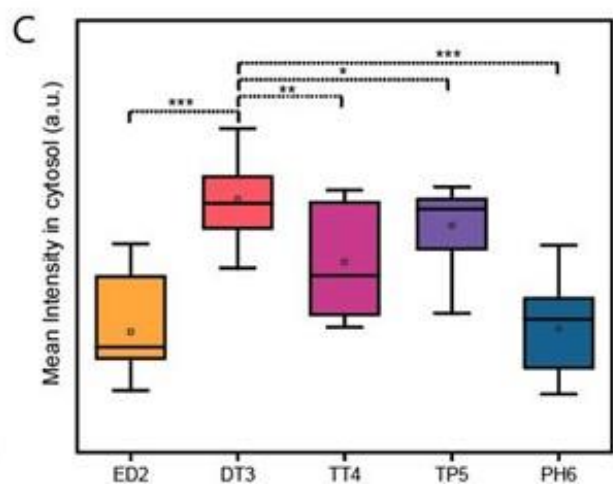
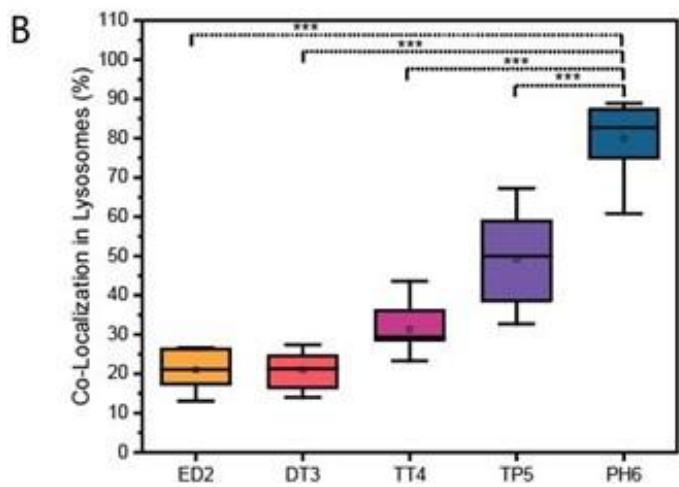
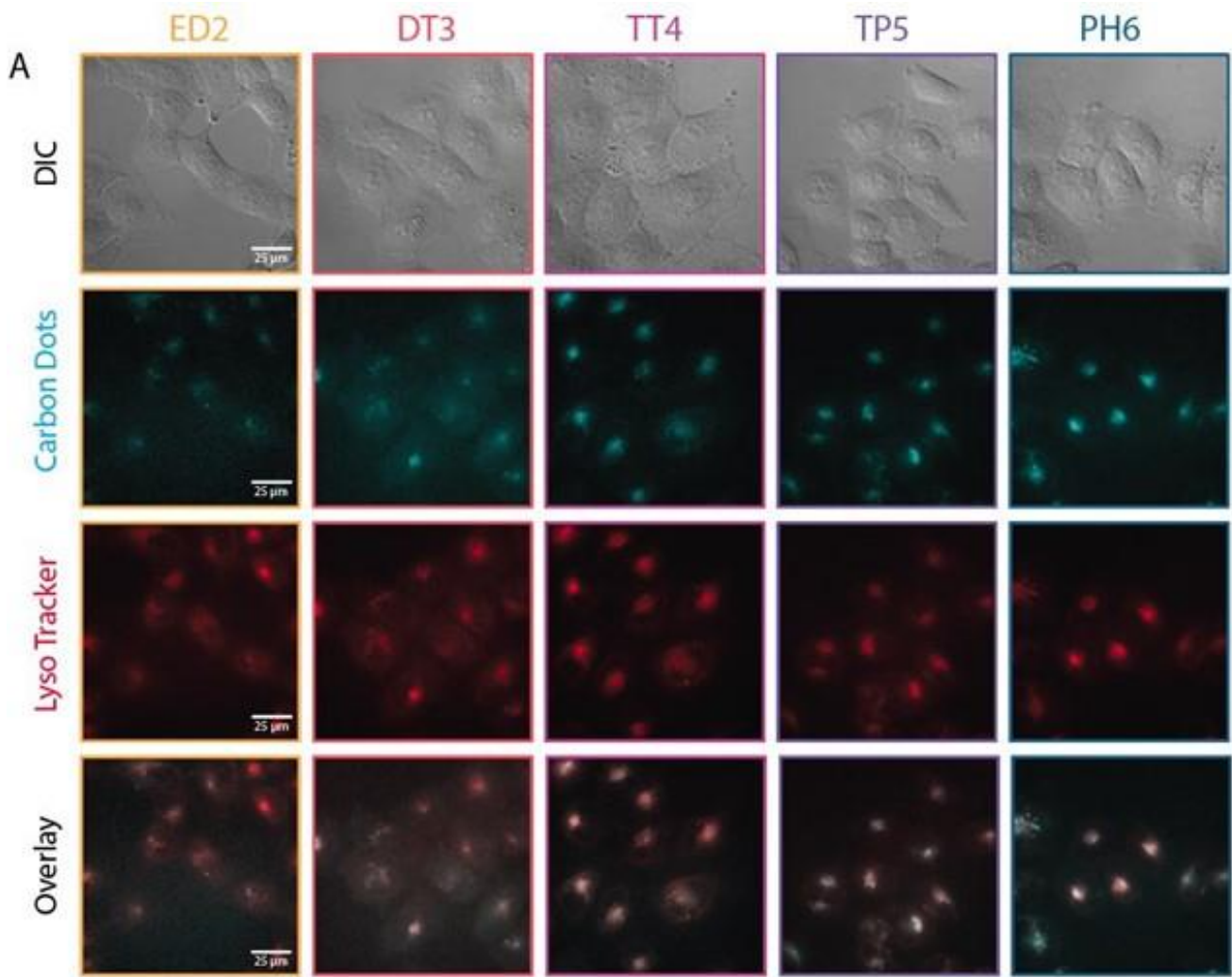


Figure 11. CDs localize to the lysosomes and cytosol in HeLa cells. (A) Brightfield (top) and fluorescence images show live HeLa cells 24 hours after treatment with 1000 ug/mL of the CDs (blue) as indicated, co-stained for lysotracker (red). The scale bar is 25 µm. (B) A box and whiskers graph show the % co-localization of CDs as indicated with lysotracker using Pearson’s correlation. Bars indicate standard deviation. One-way ANOVA and paired t-tests to PH6 were done to show significance (** $p < 0.001$). (C) A box and whiskers graph shows the mean intensity (a.u.) of CDs in the cytosol. Bars indicate standard deviation. A one-way ANOVA and paired t-tests to DT3 were done to show significance (* $p < 0.05$; ** $p < 0.01$; *** $p < 0.001$).

Chapter 4. Discussion

CDs have optical properties that could make them ideal for diagnostic imaging applications at the cellular level. While quantum dots also have ideal optical properties, they often contain metals or other toxic reagents and lack biocompatibility. Since CDs are typically synthesized using organic materials, they are predicted to have improved biocompatibility. However, few studies have assessed CDs properly and/or thoroughly at the cellular level, and the impact of specific changes in their physicochemical properties on uptake and localization is not well understood. Here, we show that an increase in amine passivation correlates with an increase in their uptake in both HeLa and HFF-1 cells. In addition, their amine passivation also correlated with an increase in lysosome localization, suggesting that PH6-CDs could be used to develop nanoproboscopes and/or to deliver specific drugs to the lysosomes. Furthermore, DT3-CDs were shown to be more strongly enriched in the cytosol compared to the other CDs. Thus, these CDs could be used as visual tool to study the mechanism of action of drugs in cells, or to deliver medicinal compounds by avoiding their entrapment in the endosomes.

Assessment of the optical and physicochemical properties of the amine-passivated CDs revealed that all amine-passivated CDs have similar excitation and emission spectra, with varying quantum yields. This suggests that amine-passivation does not dramatically impact their optical properties, but the organization of the nitrogen doped to the surface and or incorporated in the carbon core can influence quantum yield. Further, PH6-CDs were shown to have the highest fluorescent signal in both cell lines, suggesting that high quantum yield, although very important, should not be a limiting factor for imaging applications. Thus, more thorough physico-chemical analyses were performed. We found that the surface properties of the different amine-passivated CDs based on elemental composition via FTIR and XPS fit with what was expected. For example, as the amine-passivation increased, the CO-O-H peaks transitioned to C=C/C=N and N-H/C-N peaks. However, there was a difference in the amides vs. amines between the different CDs. These differences can be explained by the molecular structure of the precursors and their incorporation to the carbon core. It is not clear if this would impact their ability to enter cells and/or subcellular localization, which could be predicted to correlate with an increase in surface charge. Indeed, with increased passivation, as the surface carboxyl converts to amides, and finally to amines, the amides functional groups decrease at the surface while the amines increase, which is in agreement with

the FTIR analysis. The increase in positively charged amines directly correlated with an increase in their surface charge with PH6-CDs having the most positive zeta-potential at + 6mV.

Assessment of cellular uptake and cytotoxicity revealed that the different amine-passivated CDs can enter both HeLa and HFF-1 cells with no or low toxicity (e.g., for those with measurable IC_{50} for toxicity was a high value in both cell types). This important finding supports our prediction that these CDs are highly biocompatible. HFF-1 cells are non-cancerous and have a different origin (fibroblasts) compared to HeLa cells (epithelial). In both cell types, we saw that the PH6-CDs had the highest signal. This could reflect that more of these CDs enter cells compared to the other CDs. Since PH6-CDs have the most positive surface charge, electrostatic interaction between the highly negative plasma membrane and the positive charge of the CDs could enhance their uptake in cells which agrees with the literature.⁴³ In addition, they could also localize preferentially to the lysosomes compared to the other CDs. Indeed, we did measure significantly stronger co-localization with these CDs and lysosomes compared to the other CDs.

There was also an increase in DT3-CDs in the cytosol of both HeLa and HFF-1 cells. This exciting finding could reveal that they can either escape the endosomal system during fusion and acidification of the maturing endosomes, or they are passively entering cells through the plasma membrane. There are several findings that support the latter hypothesis. First, all of the CDs are too small to enter cells through clathrin or caveolin-dependent endocytosis, and likely enter through micropinocytosis or a less-selective mechanism^{46,47}. Further, based on their elemental composition and surface properties, DT3-CDs could be predicted to have amphiphilic properties, which could permit them to more directly interact with the lipid microenvironment. In support of this, while they are dispersed in aqueous solutions at low concentrations, they aggregate at higher concentrations which is not observed for other CDs, suggesting they have ‘some’ hydrophobic properties (**Appendix 1.2**).

The different types of amine-passivation generate CDs with different properties that could make them useful for different applications. Since PH6-CDs are bright and strongly localize to the lysosomes, these CDs could be used for applications that require lysosome-specific sensing or delivery. In addition, their remarkable photostability, high quantum yield and low PDI makes them great candidates as bioimaging nanotools. Similarly, the DT3-CDs could be useful for applications that require sensing and/or delivery to the cytosol.

Most currently synthesized CDs emit in the blue region, with potential use for cellular-based studies. Fluorescence microscopy is commonly used for cell biological studies and relies on the use of probes in the visible light spectrum which span from 350nm to 700nm. Many stains, dyes, probes, and fluorescent proteins take advantage of the UV-vis region for imaging of biological processes, organelles, and subcellular structures. Examples of commonly used blue-fluorescent dyes include DAPI and Hoechst to image chromatin, and have been extremely important in revealing mechanisms controlling key cellular processes.⁴⁸ Since most CDs fluoresce in the blue region, depending on their subcellular localization and ability to be targeted to specific organelles, they could be designed as novel bioimaging tools.^{20,22,49} In addition, there are reports of CDs with emission wavelengths that include the NIR which is more suitable for tissue-based bioimaging applications. Imaging in the NIR regions allows for deeper tissue penetration, low autofluorescence and a lower signal-to-noise ratio, and CDs with NIR emission could become useful for diagnostic applications.^{29,50} In particular, the ability of these dots to sense changes in temperature could be used for the diagnosis of diseases such as inflammation and cancer at the cellular level, since changes in metabolic activity and/or mechanisms can cause a change in temperature.^{27,51} Further, CDs that sense changes in pH within late endosomes or lysosomes could be useful in the diagnosis of pathologies that affect these organelles, such as neurodegenerative diseases.^{32,52} However, before CDs can be used for medical applications, more work needs to be done to determine their biocompatibility at the tissue/whole organism-level with more knowledge of targeting mechanisms.

Chapter 5. References

1. Online VA, Homepage J. 2008 Gold : Chemistry , Materials and Catalysis Issue Please take a look at the full table of contents to access the. 2008.
2. Ding S, Lyu Z, Li S, et al. Molecularly imprinted polypyrrole nanotubes based electrochemical sensor for glyphosate detection. *Biosens Bioelectron.* 2021;191. doi:10.1016/j.bios.2021.113434
3. Nakhaei P, Margiana R, Bokov DO, et al. Liposomes: Structure, Biomedical Applications, and Stability Parameters With Emphasis on Cholesterol. *Front Bioeng Biotechnol.* 2021;9(September):1-23. doi:10.3389/fbioe.2021.705886
4. Danaei M, Dehghankhold M, Ataei S, et al. Impact of particle size and polydispersity index on the clinical applications of lipidic nanocarrier systems. *Pharmaceutics.* 2018;10(2):1-17. doi:10.3390/pharmaceutics10020057
5. Erogbogbo F, Chang C, Yong K, et al. Bioconjugation of Luminescent Silicon Quantum Dots for Selective Uptake by Cancer Cells. 2011:1081-1088.
6. Rabouw FT, Donega CM. Excited-State Dynamics in Colloidal Semiconductor. *Top Curr Chem.* 2016;374(5):1-30. doi:10.1007/s41061-016-0060-0
7. Reshma VG, Mohanan P V. Quantum dots : Applications and safety consequences. 2019;205(July 2018):287-298. doi:10.1016/j.jlumin.2018.09.015
8. Geoffrion LD. Journal of Physics and Chemistry of Solids Quantum confinement : Size on the grill ! 2020;140(December 2019). doi:10.1016/j.jpccs.2019.109320
9. Rojas-Gutierrez PA, Bekah D, Seuntjens J, Dewolf C, Capobianco JA. Cellular Uptake, Cytotoxicity and Trafficking of Supported Lipid-Bilayer-Coated Lanthanide Upconverting Nanoparticles in Alveolar Lung Cancer Cells. *ACS Appl Bio Mater.* 2019;2(10):4527-4536. doi:10.1021/acsabm.9b00649
10. Dong H, Du S, Zheng X, et al. Lanthanide Nanoparticles : From Design toward Bioimaging and Therapy. 2015. doi:10.1021/acs.chemrev.5b00091

11. Stochaj U, Burbano CR, Cooper DR. nanoparticles on cancer cell biomarkers †. 2018;14464-14471. doi:10.1039/c8nr01451e
12. Xu X, Ray R, Gu Y, et al. Electrophoretic Analysis and Purification of Fluorescent Single-Walled Carbon Nanotube Fragments. 2004;12736-12737.
13. Liu H, Ye T, Mao C. Fluorescent carbon nanoparticles derived from candle soot. *Angew Chemie - Int Ed.* 2007;46(34):6473-6475. doi:10.1002/anie.200701271
14. Wang D, Wang Z, Zhan Q, et al. Facile and Scalable Preparation of Fluorescent Carbon Dots for Multifunctional Applications. *Engineering.* 2017;3(3):402-408. doi:10.1016/J.ENG.2017.03.014
15. Du F, Li J, Hua Y, et al. Multicolor nitrogen-doped carbon dots for live cell imaging. *J Biomed Nanotechnol.* 2015;11(5):780-788. doi:10.1166/jbn.2015.2008
16. De Medeiros T V., Manioudakis J, Noun F, Macairan JR, Victoria F, Naccache R. Microwave-assisted synthesis of carbon dots and their applications. *J Mater Chem C.* 2019;7(24):7175-7195. doi:10.1039/c9tc01640f
17. Gharat PM, Chethodil JM, Srivastava AP, Praseetha PK, Pal H, Dutta Choudhury S. An insight into the molecular and surface state photoluminescence of carbon dots revealed through solvent-induced modulations in their excitation wavelength dependent emission properties. *Photochem Photobiol Sci.* 2019;18(1):110-119. doi:10.1039/C8PP00373D
18. Macairan JR, de Medeiros T V., Gazzetto M, Yarur Villanueva F, Cannizzo A, Naccache R. Elucidating the mechanism of dual-fluorescence in carbon dots. *J Colloid Interface Sci.* 2022;606:67-76. doi:10.1016/j.jcis.2021.07.156
19. Yang ST, Wang X, Wang H, et al. Carbon dots as nontoxic and high-performance fluorescence imaging agents. *J Phys Chem C.* 2009;113(42):18110-18114. doi:10.1021/jp9085969
20. Mahmoudian J, Hadavi R, Jeddi-Tehrani M, et al. Comparison of the photobleaching and photostability traits of Alexa fluor 568- and fluorescein isothiocyanate- conjugated antibody. *Cell J.* 2011;13(3):169-172.

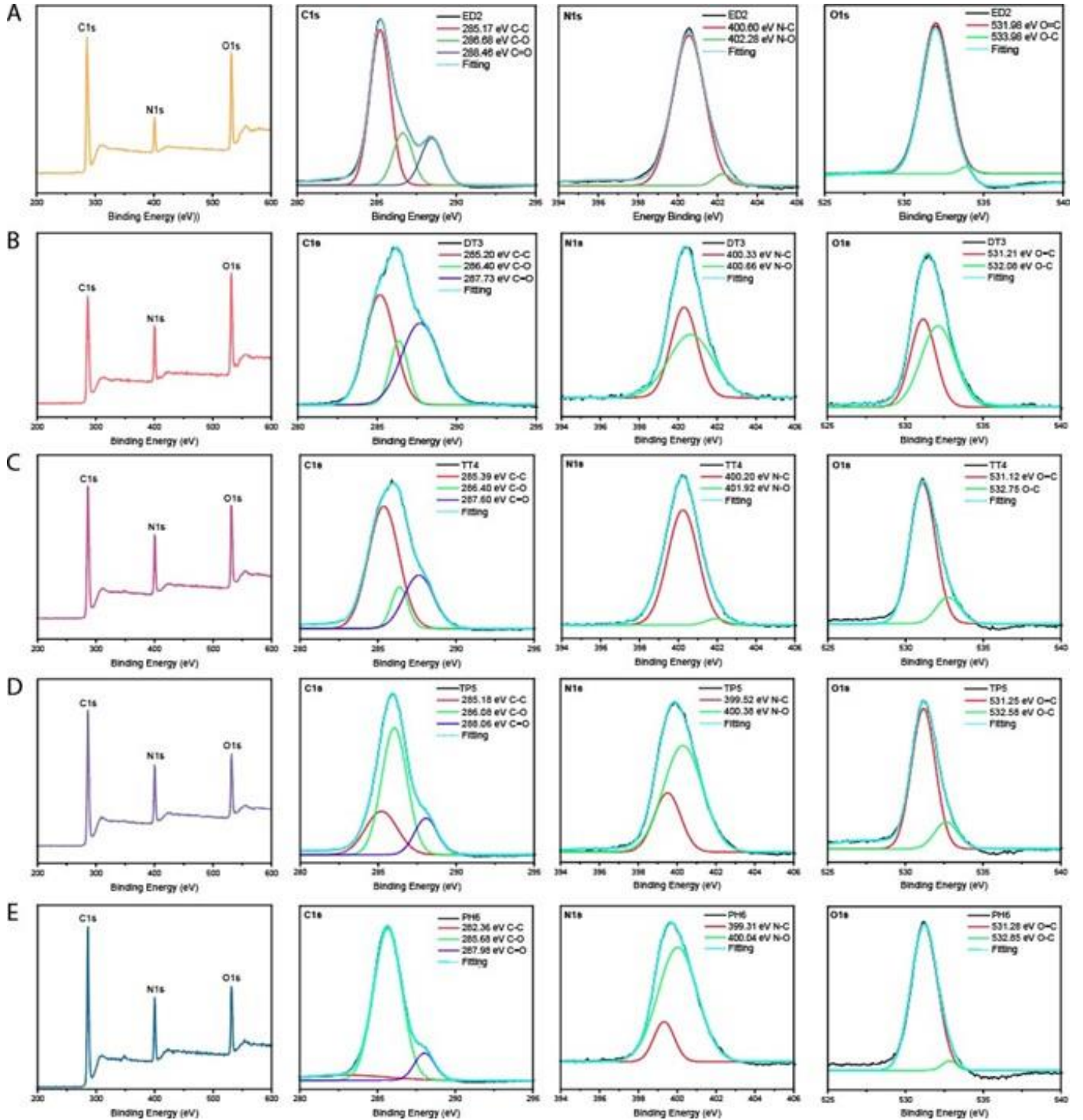
21. Wu ZL, Gao MX, Wang TT, Wan XY, Zheng LL, Huang CZ. A general quantitative pH sensor developed with dicyandiamide N-doped high quantum yield graphene quantum dots. *Nanoscale*. 2014;6(7):3868-3874. doi:10.1039/c3nr06353d
22. Manioudakis J, Victoria F, Thompson CA, et al. Effects of nitrogen-doping on the photophysical properties of carbon dots. *J Mater Chem C*. 2019;7(4):853-862. doi:10.1039/c8tc04821e
23. Ng SM. *Carbon Dots as Optical Nanoprobes for Biosensors*. Elsevier Inc.; 2019. doi:10.1016/b978-0-12-813900-4.00012-9
24. Baptista FR, Belhout SA, Giordani S, Quinn SJ. Recent developments in carbon nanomaterial sensors. *Chem Soc Rev*. 2015;44(13):4433-4453. doi:10.1039/c4cs00379a
25. Sun X, Lei Y. Fluorescent carbon dots and their sensing applications. *TrAC - Trends Anal Chem*. 2017;89:163-180. doi:10.1016/j.trac.2017.02.001
26. Liu J, Li R, Yang B. Carbon Dots: A New Type of Carbon-Based Nanomaterial with Wide Applications. *ACS Cent Sci*. 2020;6(12):2179-2195. doi:10.1021/acscentsci.0c01306
27. Macairan JR, Jaunky DB, Piekny A, Naccache R. Intracellular ratiometric temperature sensing using fluorescent carbon dots. *Nanoscale Adv*. 2019;1(1):105-113. doi:10.1039/c8na00255j
28. Lee YH, Han W, Kim Y, Kim B. Facial feature extraction using an active appearance model on the iPhone. *Proc - 2014 8th Int Conf Innov Mob Internet Serv Ubiquitous Comput IMIS 2014*. 2014:196-201. doi:10.1109/IMIS.2014.24
29. Hu S, Trinchì A, Atkin P, Cole I. Tunable photoluminescence across the entire visible spectrum from carbon dots excited by white light. *Angew Chemie - Int Ed*. 2015;54(10):2970-2974. doi:10.1002/anie.201411004
30. Zhao QL, Zhang ZL, Huang BH, Peng J, Zhang M, Pang DW. Facile preparation of low cytotoxicity fluorescent carbon nanocrystals by electrooxidation of graphite. *Chem Commun*. 2008;(41):5116-5118. doi:10.1039/b812420e
31. Ray SC, Saha A, Jana NR, Sarkar R. Fluorescent carbon nanoparticles: Synthesis,

- characterization, and bioimaging application. *J Phys Chem C*. 2009;113(43):18546-18551. doi:10.1021/jp905912n
32. Macairan JR, Zhang I, Clermont-Paquette A, Naccache R, Maysinger D. Ratiometric pH Sensing in Living Cells Using Carbon Dots. *Part Part Syst Charact*. 2020;1900430:1-7. doi:10.1002/ppsc.201900430
 33. Vasimalai N, Vilas-boas V, Gallo J, et al. Green synthesis of fluorescent carbon dots from spices for in vitro imaging and tumour cell growth inhibition. 2018:530-544. doi:10.3762/bjnano.9.51
 34. Li Q, Ohulchansky TY, Liu R, et al. Photoluminescent carbon dots as biocompatible nanoprobes for targeting cancer cells in vitro. *J Phys Chem C*. 2010;114(28):12062-12068. doi:10.1021/jp911539r
 35. Manzanares D, Ceña V. Endocytosis: The nanoparticle and submicron nanocompounds gateway into the cell. *Pharmaceutics*. 2020;12(4):1-22. doi:10.3390/pharmaceutics12040371
 36. Zhou N, Zhu S, Maharjan S, et al. Elucidating the endocytosis, intracellular trafficking, and exocytosis of carbon dots in neural cells. *RSC Adv*. 2014;4(107):62086-62095. doi:10.1039/c4ra09525a
 37. Foroozandeh P, Aziz AA. Insight into Cellular Uptake and Intracellular Trafficking of Nanoparticles. *Nanoscale Res Lett*. 2018;13. doi:10.1186/s11671-018-2728-6
 38. Behzadi S, Serpooshan V, Tao W, et al. Cellular uptake of nanoparticles: Journey inside the cell. *Chem Soc Rev*. 2017;46(14):4218-4244. doi:10.1039/c6cs00636a
 39. Santos T, Varela J, Lynch I, Salvati A, Dawson KA. Effects of Transport Inhibitors on the Cellular Uptake of Carboxylated Polystyrene Nanoparticles in Different Cell Lines. 2011;6(9). doi:10.1371/journal.pone.0024438
 40. Chithrani BD, Ghazani AA, Chan WCW. Determining the size and shape dependence of gold nanoparticle uptake into mammalian cells. *Nano Lett*. 2006;6(4):662-668. doi:10.1021/nl052396o

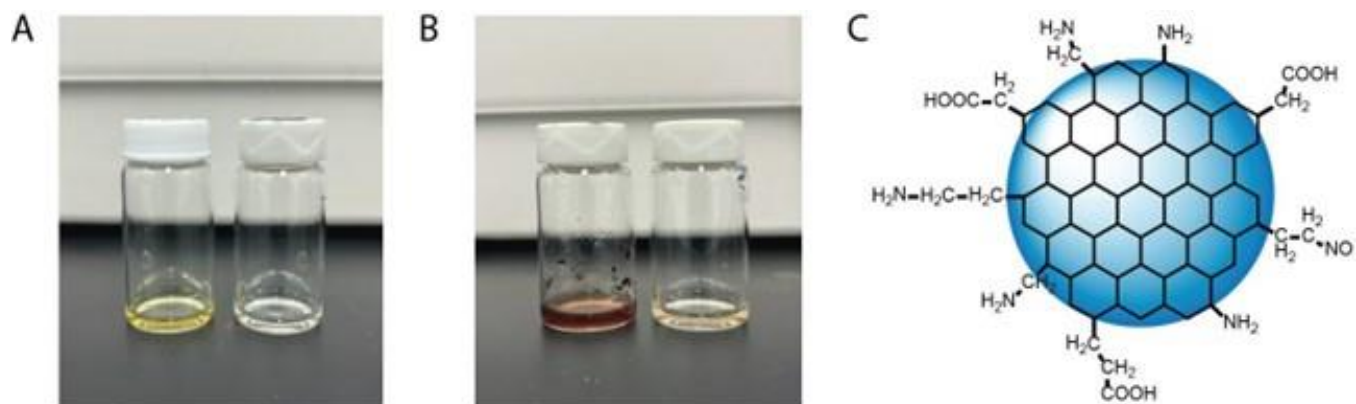
41. Shan Y, Ma S, Nie L, et al. Size-dependent endocytosis of single gold nanoparticles. *Chem Commun.* 2011;47(28):8091-8093. doi:10.1039/c1cc11453k
42. Xu ZP, Niebert M, Porazik K, et al. Subcellular compartment targeting of layered double hydroxide nanoparticles. *J Control Release.* 2008;130(1):86-94. doi:10.1016/j.jconrel.2008.05.021
43. Dausend J, Musyanovych A, Dass M, et al. Uptake mechanism of oppositely charged fluorescent nanoparticles in Hela cells. *Macromol Biosci.* 2008;8(12):1135-1143. doi:10.1002/mabi.200800123
44. Tao W, Zeng X, Wu J, et al. Polydopamine-based surface modification of novel nanoparticle-aptamer bioconjugates for in vivo breast cancer targeting and enhanced therapeutic effects. *Theranostics.* 2016;6(4):470-484. doi:10.7150/thno.14184
45. Jiang X, Dausend J, Hafner M, et al. Specific Effects of Surface Amines on Polystyrene Nanoparticles in their Interactions with Mesenchymal Stem Cells. *Nanoscale.* 2010;3(5):2028-2035. doi:https://doi.org/10.1021/bm901348z
46. Roduner E. Size matters: Why nanomaterials are different. *Chem Soc Rev.* 2006;35(7):583-592. doi:10.1039/b502142c
47. Shang L, Nienhaus K, Nienhaus GU. Engineered nanoparticles interacting with cells: Size matters. *J Nanobiotechnology.* 2014;12(1):1-11. doi:10.1186/1477-3155-12-5
48. Karg TJ, Golic KG. Photoconversion of DAPI and Hoechst dyes to green and red-emitting forms after exposure to UV excitation. 2018:235-245.
49. Li H, Yan X, Kong D, et al. Recent advances in carbon dots for bioimaging applications. *Nanoscale Horizons.* 2020;5(2):218-234. doi:10.1039/c9nh00476a
50. Hang Y, Boryczka J, Wu N. Visible-light and near-infrared fluorescence and surface-enhanced Raman scattering point-of-care sensing and bio-imaging: A review. *Chem Soc Rev.* 2022;51(1):329-375. doi:10.1039/c9cs00621d
51. Yu P, Wen X, Toh YR, Tang J. Temperature-dependent fluorescence in carbon dots. *J Phys Chem C.* 2012;116(48):25552-25557. doi:10.1021/jp307308z

52. Colacurcio DJ, Nixon RA. Disorders of lysosomal acidification—The emerging role of v-ATPase in aging and neurodegenerative disease. *Ageing Res Rev.* 2016;32:75-88. doi:10.1016/j.arr.2016.05.004

Appendix 1



1.1 XPS survey spectrum of all CDs showcasing 3 binding energies ascribed to C1s, N1s and O1s (A) XPS survey and deconvoluted spectra for ED2-CDs; (B) XPS survey and deconvoluted spectra for DT3-CDs; (C) XPS survey and deconvoluted spectra for TT4-CDs; (D) XPS survey and deconvoluted spectra for TP5-CDs; (E) XPS survey and deconvoluted spectra for PH6-CDs



1.2. (A) PH6-CDs aqueous dispersion. On the left (more yellow solution) PH6-CDs were dispersed at a final concentration of 5 mg/mL. on the right (light yellow solution) PH6-CDs were dispersed at a final concentration of 0.5 mg/mL; (B) DT3-CDs aqueous dispersion. On the left (dark brown solution) DT3-CDs were dispersed at a final concentration of 5 mg/mL. on the right (light brown solution) DT3-CDs were dispersed at a final concentration of 0.5 mg/mL; (C) Diagram of the suggested amphiphilic DT3-CDs structure showing non-polar aliphatic hydrophobic CH_2 groups linked to hydrophilic carboxyl, amides, and amines functional groups.

Table 1. One-Way ANOVA and Paired t-test statistical analysis for cellular uptake of CDs in both HeLa and HFF-1 cells for **Fig.9**

Statistical Test	Cell Line	Groups	P-value	Data Interpretation
One-way ANOVA	HeLa	ED2	1.76E ⁻³²	Population means are significantly different
		DT3		
		TT4		
		TP5		
		PH6		
Paired t-test	HeLa	ED2:PH6	1.33E ⁻⁹	Population means are significantly different
		DT3:PH6	1.81E ⁻⁹	Population means are significantly different
		TT4:PH6	1.09E ⁻⁹	Population means are significantly different
		TP5:PH6	5.58E ⁻⁷	Population means are significantly different
One-way ANOVA	HFF-1	ED2	7.40E ⁻⁸	Population means are significantly different
		DT3		
		TT4		
		TP5		
		PH6		
Paired t-test	HFF-1	ED2:PH6	3.69E ⁻⁴	Population means are significantly different
		DT3:PH6	7.78E ⁻⁷	Population means are significantly different
		TT4:PH6	4.01E ⁻⁵	Population means are significantly different
		TP5:PH6	6.47E ⁻⁵	Population means are significantly different

Table 2. One-Way ANOVA and Paired t-test statistical analysis for Lysosome and Cytosol co-localization of CDs in HFF-1 cells for **Fig.10**

Statistical Test	Co-Localization	Groups	P-value	Data Interpretation
One-way ANOVA	Lysosome	ED2	3.80E ⁻³²	Population means are significantly different
		DT3		
		TT4		
		TP5		
		PH6		
Paired t-test	Lysosome	ED2:PH6	9.71E ⁻¹⁰	Population means are significantly different
		DT3:PH6	6.10E ⁻¹⁰	Population means are significantly different
		TT4:PH6	3.01E ⁻⁸	Population means are significantly different
		TP5:PH6	1.83E ⁻⁴	Population means are significantly different
One-way ANOVA	Cytosol	ED2	1.46E ⁻¹¹	Population means are significantly different
		DT3		
		TT4		
		TP5		
		PH6		
Paired t-test	Cytosol	ED2:PH6	2.36E ⁻⁸	Population means are significantly different
		DT3:PH6	1.45E ⁻⁶	Population means are significantly different
		TT4:PH6	1.44E ⁻⁴	Population means are significantly different
		TP5:PH6	7.78E ⁻⁷	Population means are significantly different

Table 3. One-Way ANOVA and Paired t-test statistical analysis for co-localization in the cytosol of CDs in both HeLa and HFF-1 cells for **Fig.11**

Statistical Test	Co-Localization	Groups	P-value	Data Interpretation
One-way ANOVA	Lysosome	ED2	3.80E ⁻³²	Population means are significantly different
		DT3		
		TT4		
		TP5		
		PH6		
Paired t-test	Lysosome	ED2:PH6	9.71E ⁻¹⁰	Population means are significantly different
		DT3:PH6	6.10E ⁻¹⁰	Population means are significantly different
		TT4:PH6	3.01E ⁻⁸	Population means are significantly different
		TP5:PH6	1.83E ⁻⁴	Population means are significantly different
One-way ANOVA	Cytosol	ED2	2.39E ⁻¹¹	Population means are significantly different
		DT3		
		TT4		
		TP5		
		PH6		
Paired t-test	Cytosol	ED2:PH6	4.64E ⁻⁵	Population means are significantly different
		DT3:PH6	0.00172	Population means are significantly different
		TT4:PH6	0.02642	Population means are significantly different
		TP5:PH6	8.83E ⁻⁵	Population means are significantly different